# Optoelectronic Quantum Telecommunications Based on Spins in Semiconductors

ELI YABLONOVITCH, H. W. JIANG, HIDEO KOSAKA, HANS D. ROBINSON, DEEPAK SETHU RAO, AND T. SZKOPEK

*Invited Paper*

*The transmission of quantum information over long distances will allow new forms of data security, based on quantum cryptography. These new technologies rely for security on the quantum "uncertainty principle" and on the long distance transmission of "quantum entanglement." A new type of telecommunications device called the "quantum repeater" can allow the faithful transmission of quantum information over worldwide distances, in spite of the inevitably severe losses while propagating along optical fibers.*

*In a quantum repeater, information is stored in the quantum state of a semiconductor electron spin, while complementary entangled information is transmitted as a photon down the optical fiber. This long-range entanglement permits the execution of the teleportation algorithm, which accurately transmits a quantum state over long distances. The quantum repeater is an excellent stepping stone to larger quantum information processors, since teleportation requires only three quantum logic gates.*

*This paper reviews the experimental status of semiconductor quantum repeaters, including the spin resonance transistor logic gates, and the experimental detection of single photons in a manner that preserves their spin information.*

***Keywords*—*Decoherence, quantum computing, quantum cryptography, quantum repeater, spin resonance transistor, spintronics, teleportation.***

## I. INTRODUCTION

There is reason to believe that quantum information may be the next logical extension to the information technology revolution. Among the many developments that motivate the manipulation of quantum information was the discovery, in 1994, of the Shor quantum algorithm for the factorization [1] of large numbers. Another important development was Bennett's idea [2] for quantum teleportation. This is a form of telecommunication, in which quantum information *is* transmitted. It would enable long distance quantum cryptography, as well as other forms of quantum-based telecommunications security.

In this paper, we will describe the prospects for manipulating quantum information in the form of spins in optoelectronic semiconductors. A quantum teleportation circuit, augmented by a new type of photodetector, becomes a quantum repeater, allowing quantum information to be safely retransmitted over long distances.

Manuscript received October 16, 2002; revised January 28, 2003. This paper was supported in part by the Defense Advanced Research Projects Agency (DARPA) and in part by the Army Research Office under Grant MDA972-99-1-0017 and Grant DAAD19-00-1-0172. The content of the information does not necessarily reflect the position or the policy of the government, and no official endorsement should be inferred.

E. Yablonovitch, H. D. Robinson, D. S. Rao and T. Szkopek are with the Electrical Engineering Department, University of California, Los Angeles, Los Angeles, CA, 90095-1594 USA.

H. W. Jiang is with the Physics Department, University of California, Los Angeles, Los Angeles, CA, 90095-1594 USA.

H. Kosaka is with the Electrical Engineering Department, University of California, Los Angeles, CA, 90095-1594 USA and also with the Fundamental Research Laboratories, NEC Corporation 34 Miyukigaoka, Tsukuba, Ibaraki 305-8501, Japan.

Digital Object Identifier 10.1109/JPROC.2003.811799

## II. THE GIANT QUANTUM REGISTER

To see the richness of quantum information it suffices to contrast the number of configurations in a quantum system compared to a classical memory. In a classical binary memory of N-bits, there are $2^{\mathrm{N}}$ possible configurations. In an analog memory, or in multilevel logic, there are slightly more configurations, $(2^{\alpha})^{\mathrm{N}}$, where $\alpha$ is the number of bits of analog precision. In a quantum system, the situation is surprisingly different. Consider the size of the wave-function of

1 spin: $|\Psi\rangle = \mathrm{c}_1|0\rangle + \mathrm{c}_2|1\rangle$

2 spins: $|\Psi\rangle = \mathrm{c}_1|00\rangle + \mathrm{c}_2|01\rangle + \mathrm{c}_3|10\rangle + \mathrm{c}_4|11\rangle$

where the $\mathrm{c_i}$ are the complex coefficients that characterize the wave function

1 spin $\rightarrow$ 2 complex numbers

2 spins $\rightarrow$ 4 complex numbers.

One might be lead to the idea that the number of complex coefficients is 2N, where N is the number of spins, or qubits. However that idea is dashed by an examination of the wave function for $\mathrm{N} = 3$ spins

3 spins $|\Psi\rangle = \mathrm{c}_1|000\rangle + \mathrm{c}_2|001\rangle + \mathrm{c}_3|010\rangle + \mathrm{c}_4|011\rangle + \mathrm{c}_5|100\rangle + \mathrm{c}_6|101\rangle + \mathrm{c}_7|110\rangle + \mathrm{c}_8|111\rangle$

3 spins $\rightarrow$ 8 complex numbers.

Further inductive reasoning leads to a general formula that N spins require a wave function with $2^{\mathrm{N}}$ complex numbers. If each complex number were described with $\alpha$ bits of analog precision then each complex quantum coefficient would have $(2^{\alpha})$ configurations, but the total number of quantum configurations for the entire wave function would be $(2^{\alpha})^{2^{\mathrm{N}}}$. This is to be contrasted with the number of configurations in classical multilevel logic $(2^{\alpha})^{\mathrm{N}}$.

Neglecting momentarily the analog precision, the overall contrast with between a classical memory and a quantum memory register is a $2^{\mathrm{N}}$ scaling versus a $2^{2^{\mathrm{N}}}$ scaling. This makes a rather substantial difference as illustrated by the following three cases.

Case a) Thirty-four spins, or qubits, or transistors. Indeed, we expect each spin qubit to be in, and controlled by, a new type of transistor. The number of quantum mechanical coefficients is $2^{34}$. If each coefficient is described by 2 bits of analog precision, (merely specifying the quadrant of the complex plane in which the coefficient resides), that leads to a wave function that requires $2^{34} \times 2^2 = 2^{36}$ classical bits to record. That amounts to 80 Gbits of data necessary to write the wave function, which amounts to 10 Gbytes which would require only one hard disk.

Case b) Sixty-one spins, or qubits, or transistors. The number of quantum mechanical coefficients is $2^{61}$. If each coefficient is described by 2 bits of analog precision as before, that leads to a wave function that requires recording $2^{61} \times 2^2 = 2^{63}$ classical bits. That amounts to $8 \times 10^{18}$ bits of data necessary to write the wave function, which would require $10^8$ hard disks. One-hundred-million hard disks is on the order of the world-wide annual production volume.

Case c) Ninety-four spins, or qubits, or transistors. The number of quantum mechanical coefficients is $2^{94}$. If each coefficient is described by 2 bits of analog precision as before, that leads to a wave function that requires $2^{94} \times 2^2 = 2^{96}$ to record. That amounts to $8 \times 10^{28}$ bits of data necessary to write the wave function, which would require $\sim 10^{18}$ hard disks. This would require $10^{10}$ years of the world-wide annual hard disk production volume. $10^{10}$ years is approximately the age of the universe!

This exponential scale-up in the implicit quantum memory register, with only a modest increase number of transistors, is characteristic of quantum information. The implicit size of a quantum register is beyond astronomical. Why is it so huge? In a classical memory each bit can be zero or one. In a quantum memory one must consider the probability of each bit being zero or one, depending on the state of all the other qubits in the system. There are $\sim 2^{\mathrm{N}}$ conditional or composite probability amplitudes for every qubit, representing all the possible entanglement configurations. That is the source of the giant quantum memory register in moderate sized systems.

This quantum register should be regarded as a giant internal "scratch-pad" to store intermediate results of very complex computations. If the computer user were to attempt to read the quantum register, the wave function would collapse, and the user would read the small number of qubits as if they were a small classical memory. Thus, quantum memory is useless for storing motion pictures or other memory intensive functions for readout. Only the computer itself can access the giant quantum register internally. At the end of a computation, the qubits are read out, and the result is a numerical factor, or a numerical pointer, or the answer to a yes/no question, that can be read out from the relatively small number of available qubits.

## III. The Quantum Repeater Algorithm

In contrast to the giant quantum register, a quantum repeater useful for telecommunications runs the relatively small teleportation algorithm [3] that requires only three qubits. A block diagram of the quantum repeater is illustrated in Fig. 1. The three horizontal lines represent the logic state of the three qubits. (The word "teleportation" is probably a misnomer, since it represents a very sophisticated telecommunication of information, rather than the physical transport of matter.)

It is quite surprising that it would be possible to safely transmit qubit information over long distances. Qubits are rather fragile, and they collapse when observed. The no-cloning theorem ensures there is no way to preserve copies of the qubits. If you directly transmit qubits, they might become absorbed in an optical fiber.

The secret to the quantum repeater is to not send qubits through a lossy optical link. Instead, one member of an entangled pair of is sent. Entangled singlet pairs of electrons are rather common, since most electrons on earth are composed of singlet pairs. Nonlinear optical parametric down conversion can also generate singlet pairs of photons. Singlet pairs carry no special quantum information, and they can be readily generated. By transmitting one member of singlet pair, there is very little risk. If it becomes lost, then another singlet pair can be created, allowing eventually for the sharing of entanglement between different locations.

A sensor must be made available, to flag the successful arrival of a photon that provides sharing of entanglement between different locations. Thus, the two key new components of a quantum repeater, over and above what is required for teleportation, are: 1) a photodetector that can flag the successful arrival of half of an entangled pair; 2) a storage element to safely store the qubit until that happens.

The storage of quantum information is an important new function. Indeed the storage must continue for a time equal to the round-trip time of the quantum data link. A round trip is required to share the entanglement and for the acknowledgment of the safe arrival of a one member of an entangled pair. In the meantime, the qubit must be stored safely, preserving its quantum coherence. A key of component in the quantum repeater block diagram is the quantum storage element.

The preservation of quantum coherence in a qubit for long time periods, is a significant new figure-of-merit in technology. In addition to its value in quantum repeaters, a long quantum coherence time results in smaller errors, that

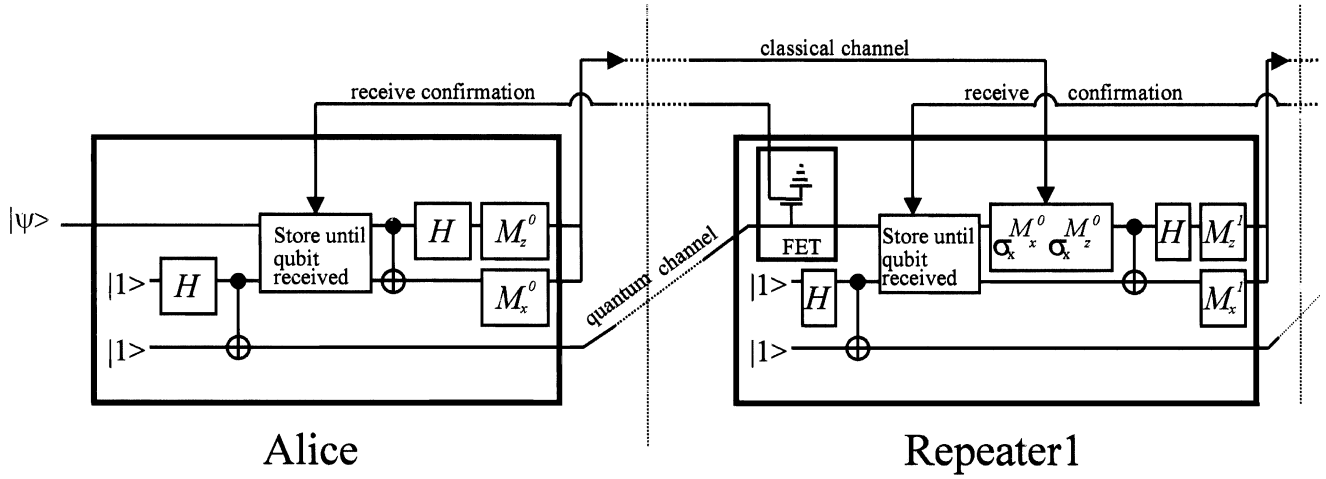


**Fig. 1.** Block diagram of the first two stages of a quantum repeater system. The algorithm requires only three qubits, represented by the three horizontal logic lines. H represents Hadamard rotations, $M_i$ represents measurement along the i axis, and $\sigma_x$ represents single-qubit rotation around the x axis. A key role is played by qubit storage, that continues until an acknowledgment signal is received from an FET photodetector in the next repeater. The FET photodetector should sense photo-charge, but not entangle the photo-electron spin state.

are more easily correctable in complex algorithms like the Shor factorization algorithm. Thus, quantum repeaters, and quantum error correction are both strong motivations for long decoherence times in quantum information processing.

## IV. Candidate Physical Systems for Quantum Information Processing

The introduction of quantum error correction [4] in 1996 began an exhaustive search for candidate physical qubits that could satisfy the requirements for a decoherence error rate of $< 10^{-4}$ within a gate operation time. Of course, atomic systems benefit from only very small coupling to the environment, and have the longest history of [5] quantum information experiments. Additionally, there has been a lot of progress in nuclear spin systems, where factorization of a small integer [6] has been demonstrated.

The main disadvantage for nuclear spin systems, in the long run, is that the clock speed would appear to be limited. For that reason, electron spin systems interacting by the potentially speedy exchange interaction [7] have begun to receive intense scrutiny. In particular, electron spins trapped in Silicon [8] were known to have very favorable [9] decoherence properties, that have been confirmed and extended in recent [10] measurements.

Simultaneously, there has been a recent breakthrough [11] in mixed flux/charge qubits in superconducting Josephson junction resonators. For the first time, the longitudinal relaxation time, $T_1$, and the transverse relaxation time, $T_2$, were distinguished [11] in a superconducting qubit.

Yet another new approach emerged [12] recently, that has been named linear optics quantum computing (LOQC). The key elements in LOQC are single photon detectors, that produce in effect, a significant nonlinear response at the level of individual photons. Postselection plays a big role here, and the success rate is low, but the required components, single photon detectors and single photon light emitting diodes [13], already exist, and merely require refinement.

Thus, there is no shortage of candidate physical systems for quantum information processing. As in most technologies, there are likely to be many options, and the ultimately preferred choice at any point in time may be based on specific secondary advantages that will be difficult to discern at the outset. Such a situation of tradeoffs is typical in engineering, and we are embarking on the age of engineered quantum information systems.

## V. Electron Spins in Silicon

Isolated electron spins in low-temperature semiconductors are now recognized to have considerable potential for storing and manipulating quantum information. One of the great advantages of a spin in a semiconductor is that it can be embedded into a transistor structure, and it can thereby lend itself to large-scale integration, as an integrated quantum information processor. Individual spins, or qubits, can receive logic commands from voltage pulses on individually addressable gate electrodes.

Before we embark on such a visionary quest, it is necessary to ask whether Nature favors such a technological outcome. Are electron spins in Silicon endowed with the particular properties that would make them useful as qubits? The most important property is the safe preservation of quantum mechanical phase information. That amounts to having a predictable spin angular momentum vector orientation in space, despite disturbances from the surroundings. There is much reason for optimism about low-temperature semiconductors as spin hosts. Spins in general are famous for rather weak coupling to surroundings. The vibrational degrees of freedom are frozen out at low temperatures, and the cold lattice itself can be regarded as a highly perfect atom trap. This is analogous to a trap for a cold atom in vacuum, but it is part of a semiconductor device structure.

It turns out that Nature has been very kind to electron spins in Silicon. The accepted technique for determining the fidelity and reproducibility of spin orientation is the

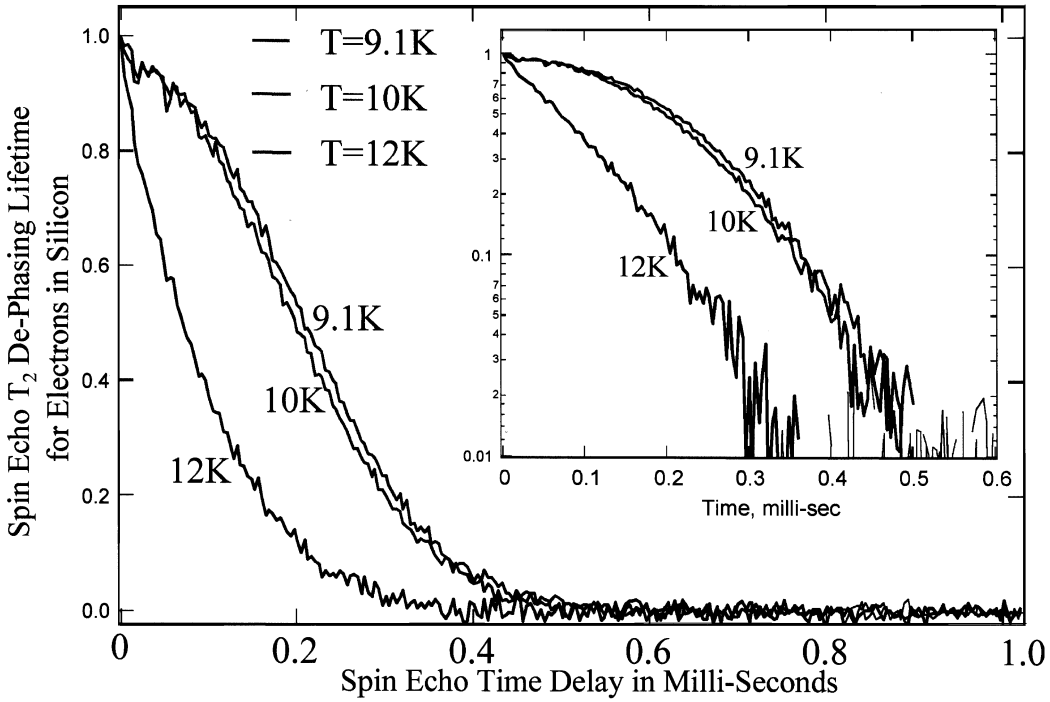


**Fig. 2.** The probability that an electron spin natural isotopic abundance Si continues to point in its original time $t = 0$ direction, after a later time t, measured by the spin echo dephasing technique. The inset is a semilog plot showing the highly nonexponential character $\sim \exp\{-t/t_o)^3\}$ of the dephasing. This nonexponential time dependence is generally associated with the spin diffusion mechanism.

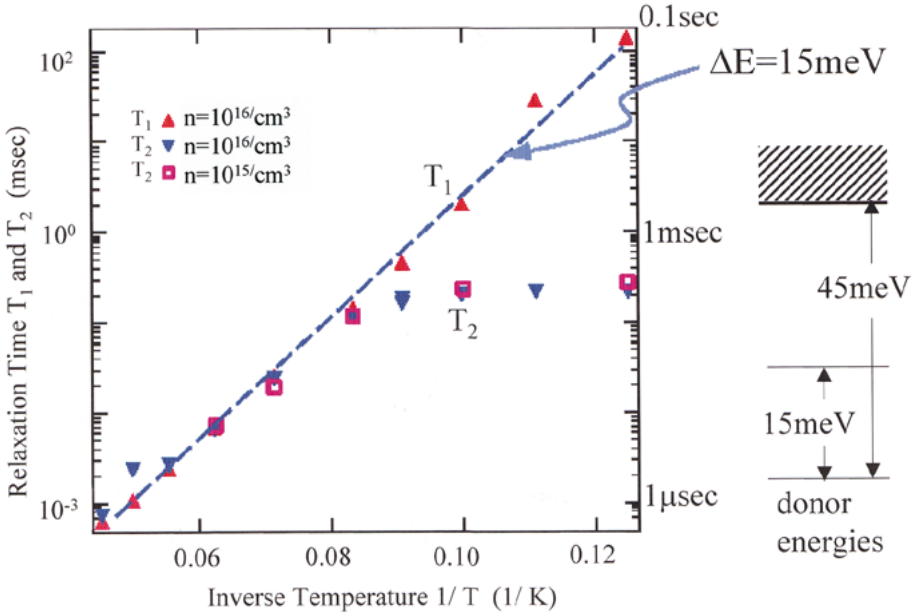


**Fig. 3.** The longitudinal $T_1$ and transverse $T_2$ relaxation times for electron spins in Silicon at low temperatures. At temperatures above 10 K, $T_1 = T_2$, with a 15 meV activation corresponding to the first excited state of the Hydrogenic donor in Si. At temperatures $<10$ K, $T_1$ continues to improve, but $T_2$ remains temperature independent $\approx$0.3 ms due to hyperfine spin diffusion. The lifetimes are hardly affected by doping level over the range tested.

spin-echo [14] method. In effect, a spin magnetic moment is left pointing is space, and then after an echo period, the probability is measured for the spin to still be pointing in the same direction. Such a probability can be written $\langle\psi|\rho|\psi\rangle$ where $|\psi\rangle$ is the initial state of the spin, and $\rho$ is the density matrix of the spin after it has interacted with the environment. The results of such a measurement are shown in Fig. 2. This probability $\langle\psi|\rho|\psi\rangle|$ is sometimes called the spin coherence, or the fidelity.

The 1/e decay lifetime in Fig. 2 becomes steadily longer with the decrease in temperature, but at temperatures of 10 K and below, there is no further improvement. A thermal activation plot at temperatures above 10 K in Fig. 3, shows that the 1/e decay lifetime follows a Boltzmann activation

dependence, with an activation energy of $\Delta E = 15$ meV. At temperatures above 10 K, the coherence lifetime $T_2$, and the population lifetime $T_1$, are both equal, and decay exponentially in time. Contrarily, at temperatures below 10 K, there is no further temperature dependence at all, and curiously the spin coherence decay is nonexponential in time, decaying as $\exp\{-(t/t_o)^\gamma\}$ where $\gamma \approx 2.25$. Thus, the mechanisms of electron spin coherence decay are quite different at temperatures above and below 10 K.

At the temperatures of this experiment, electrons are frozen out, i.e., bound to the donor ion. The Boltzmann activation energy $\Delta E = 15$ meV happens to coincide with the first excited state energy of the donor, to be compared with the $\Delta E = 45$ meV donor ionization energy. The excited state represents a distinct superposition of the six conduction band minima, different from the perfectly symmetrical ground state. Since the g-factor is actually a g-tensor, fluctuations among the differently oriented conduction band minima produce fluctuations in the Zeeman splitting that can cause both decoherence $T_2$ and population decay $T_1$. Interestingly, the population decay $T_1$ continues to follow the Boltzmann Law at low temperatures.

At low temperatures <10 K, the spin decoherence experiences a nonexponential, temperature-independent, decay mechanism. Random *phase* jumps are known to produce exponential decay. On the other hand, random *frequency* jumps produce a nonexponential $\exp\{-(t/t_o)^\gamma\}$ decay process. This $\exp\{-(t/t_o)^\gamma\}$ dependence was already well understood in the first paper [14] on spin-echoes and is known to result from nuclear spin diffusion induced, hyperfine, frequency jumps.[1] The only nuclear spin available for this mechanism is the spin $1/2$ $Si^{29}$ nucleus that is present at 5% abundance in natural Si. Indeed, in the first measurements on isotopically purified $Si^{28}$ that were published [9] in 1958, the 1/e lifetime improved by a factor 2 compared with natural Si.

We are motivated then to look for electron spin hosts, in which there are no nuclear spins present. Table 1 is an abbreviated "Periodic Table" that shows the concentration of spinless nuclei in the central columns of the periodic table. It is clear that this hyperfine induced mechanism, that dominates electron spin decoherence at low temperatures, can be eliminated by sufficient isotopic purification of the electron spin host. $Si^{28}$ of 99.99% purity is commercially obtainable.

Since each electron in a macroscopic sample sees its own specific nuclear spin environment, there is a substantial inhomogeneous spread in electron spin resonance frequencies, around a central frequency that can be 50–60 GHz in a ~2-tesla magnetic field. Spin echo measures the homogeneous lifetime of individual members of an inhomogeneous ensemble. Table 2 is a summary of these 1/e lifetimes for trapped and mobile electrons in Si, but there is no inhomogeneous broadening for mobile electrons since they rapidly average over their environment while moving.

Considerable knowledge has been accumulated regarding spin coherence of electrons in the III–V semiconductors due to Awschalom's work [15], among others. A rough survey is illustrated in Table 3. The III–V's have no spin-free nuclear isotopes whatsoever, and their decoherence lifetimes are generally shorter than the group IV semiconductors. There currently exists no knowledge of the homogeneous lifetime of electrons trapped in III–V semiconductors. To keep the electrons trapped locally, below the metal/insulator transition, requires a very low electron density. At such low concentrations, techniques like spin echo have insufficient signal strength. In any case, the high concentration of nuclear spins makes it unlikely that the homogeneous $T_2$ of trapped electrons in III–V's approaches the excellent performance in natural Si, let alone isotopically purified Si.

[1]Interestingly, these frequency fluctuations are unable to cause population transitions between Zeeman levels, and they do not contribute to T1 relaxation. Such population relaxation continues to be exponential and Boltzmann-activated, even at low temperatures; see Fig. 3

**Table 1**
In the Chart of the Nuclides, There are No Spin Zero Nuclei in Column III or Column V of the Periodic Table. In Column IV, There are Many Opportunities to Produce a Nuclear-Spin-Free Electron Host, by Isotopic Purification

| III | IV | V |
|---|---|---|
| 5 $B^{11}$ | 6 $C^{12}$ 99% spinless | 7 $N^{14}$ |
| 13 $Al^{27}$ | 14 $Si^{28}$ 95% spinless | 15 $P^{31}$ |
| 31 $Ga^{69}$ | 32 $Ge^{74}$ 92% spinless | 33 $As^{27}$ |
| 49 $In^{115}$ | 50 $Sn^{120}$ | 51 $Sb^{121}$ |

**Table 2**
The 1/e Homogeneous $T_2$ Lifetime and the Inhomogeneous $T_2^*$ Lifetime of the Electron Spin in Silicon. In Practice, the Decoherence is Nonexponential in Time. This Dephasing and Decoherence Process is Dominated by Hyperfine Interactions in Low-Temperature Silicon. Mobile Electrons See a Rapidly Changing Nuclear Spin Environment Which Averages, Producing Only Homogeneous Broadening

| Electron Spins in **Silicon** at low temps | | |
|---|---|---|
| | Homogeneous dephasing time $T_2$ | Inhomogeneous dephasing time $T_2^*$ |
| Trapped electrons | 0.3msec-0.5msec Spin Echo in n-Si | 100nsec-1μsec ESR in n-Si |
| Mobile electrons | 100nsec-10μsec magneto-resistive ESR in 2d Si-Ge electron-gas | No Inhomogeneous Broadening |

**Table 3**
Representative Homogeneous and Inhomogeneous Electron Spin Decoherence Times Among the III–V Semiconductors. Spin Echo has not been Successful for Trapped Electrons in n-GaAs since the Concentration must be Kept Very Low, to Avoid the Electrons Becoming Mobile in a Mott Transition. Generally the lifetimes are Much Shorter Than in Group IV Semiconductors

| Electron Spins in **III-V's** at low temps | | |
|---|---|---|
| | Homogeneous dephasing time $T_2$ | Inhomogeneous dephasing time $T_2^*$ |
| Trapped electrons | Not Known! Spin Echo in very lightly doped n-GaAs, to avoid exchange interactions | ≈3nsec ESR in n-GaAs |
| Mobile Electrons | 0.1nsec-500nsec (a) Awschalom et al, optical ESR (b) magneto-resistive ESR in 2-d e-gas | No Inhomogeneous Broadening |

**Table 4**
A Number of Electron Spin Hosts Perform Particularly Well at Temperatures as High as 300 K. Among These Electron Spin Hosts, Elemental Carbon in the Form of $C_{60}$ and Diamond Performs Particularly Well

| Material | temperature | $T_2$ |
|---|---|---|
| γ-irradiated quartz | 300K | 2-5 μsec |
| N-V centers in diamond, (*price/purity dependent*) | 300K | 2-100 μsec |
| N@$C_{60}$ (spin 3/2) | 300K solution | 120 μsec |
| Phosphorus in Si | <12°K | 250 μsec |

Among electron spin hosts, elemental carbon has some remarkably long decoherence times, as measured by spin echo. Table 4 shows some of these lifetimes in $C_{60}$, diamond, and for comparison at a defect center in quartz, and in n-Si. From the activation energy in Fig. 3, it is clear that more tightly bound electrons would have to be cooled to 10 K as in Si. In fact the decoherence times are longer than 0.1 ms in both $C_{60}$ and diamond. Elemental carbon has the following advantages: 1) Low atomic number and, thus, less spin-orbit coupling; 2) High Debye temperature and, thus, fewer phonons to disturb the spins; and 3) only 1% $C^{13}$. Thus, elemental carbon may be the preferred spin host for future room temperature electronic qubits.

## VI. Initial Stages of Non-Exponential Coherence Decay

For the purposes of quantum information, we do not have the luxury to wait for the 1/e decoherence time. An initial slight loss of coherence between the two spin 1/2 electron states can already be fatal. To be compatible with quantum error correction, for example, decoherence to the 0.9999 level can already [16] become problematic. Thus, we must examine the very initial stages of the decoherence process.

The electron spin frequency changes, associated with nuclear spin diffusion, cause a slow initial drift in phase. The cosine of the phase shift hardly deviates from unity, consistent with the zero initial slope in the semilog inset of Fig. 2, $(\mathrm{d}/\mathrm{dt})[\exp\{-(\mathrm{t}/\mathrm{t_o})^{\gamma}\}] = 0$. Seemingly then, we are protected from decoherence at the initial stages. On the other hand, frequency jumps and phase shifts are not the only possible sources of decoherence; as the following discussion shows:

The primary mechanism for decoherence of electron spin states, is their interaction with nuclear spins. If the nuclear spins sense, in any way, the relative up and down orientation of the electron spin, they become entangled with the electron spin Zeeman levels, destroying [17] the quantum coherence. We distinguish between entanglement induced "*decoherence*," that is in addition to frequency drift and phase shift induced "*dephasing*."

This can be made more exact by considering the global electron/nucleus wave function. They may start out at time $\mathrm{t} = 0$ as a disentangled global product wave function

$$|\Psi\rangle = |\psi\rangle\,|\phi_{\mathrm{N}}(0)\rangle = \{\mathrm{c}_0|0\rangle + \mathrm{c}_1|1\rangle\}\,|\phi_{\mathrm{N}}(0)\rangle$$

where $|\psi\rangle = \mathrm{c}_0|0\rangle + \mathrm{c}_1|1\rangle$ is the initial state of the wave function, $|0\rangle$ and $|1\rangle$ represent the two electron spin states of the qubit, and $|\phi_{\mathrm{N}}(0)\rangle$ represents the nuclear spin state at $\mathrm{t} = 0$. With the passage of time the global wave function evolves as follows:

$$|\Psi\rangle = \mathrm{c}_0|0\rangle\,|\phi_{\mathrm{N0}}(\mathrm{t})\rangle + \mathrm{c}_1|1\rangle\,|\phi_{\mathrm{N1}}(\mathrm{t})\rangle$$

where the nuclear state can evolve quite differently, depending on whether the electron spin qubit is in state $|0\rangle$ or $|1\rangle$. The reduced density matrix $\rho$ of the electron spin is obtained by tracing the global density matrix $|\Psi\rangle\langle\Psi|$ over the nuclear spin degrees of freedom. The decoherence is monitored by the off-diagonal terms in the density matrix

$$\rho_{01} = \{\mathrm{c}_0^*\mathrm{c}_1\}\,\langle\phi_{\mathrm{N0}}(\mathrm{t})|\phi_{\mathrm{N1}}(\mathrm{t})\rangle\,.$$

In the absence of hyperfine coupling, the result would be $\{\mathrm{c}_0^*\mathrm{c}_1\}$, but the presence of the nuclear spin diminishes the off-diagonal electron spin component by a factor consisting of the nuclear matrix element $\langle\phi_{\mathrm{N0}}(\mathrm{t})|\phi_{\mathrm{N1}}(\mathrm{t})\rangle$. The following two subcases emerge.

Case 1) Pure dephasing case: If $|\phi_{\mathrm{N0}}(\mathrm{t})\rangle = \mathrm{e}^{\mathrm{i}\theta}|\phi_{\mathrm{N1}}(\mathrm{t})\rangle$, and the matrix element $|\langle\phi_{\mathrm{N0}}(\mathrm{t})|\phi_{\mathrm{N1}}(\mathrm{t})\rangle| = 1$, where $\theta$ is a relative phase shift, then the global wave function can still be factored into a nuclear part and an electron spin part, and the nuclear spin is not entangled with the electron spin. There remains dephasing by the factor $\mathrm{e}^{\mathrm{i}\theta}$; $\rho_{01} = \{\mathrm{c}_0^*\mathrm{c}_1\}\mathrm{e}^{\mathrm{i}\theta}$, where $\theta$ might become a random variable depending on the details of the nuclear spin dynamics.

Case 2) Entanglement decoherence case: $|\phi_{\mathrm{N0}}(\mathrm{t})\rangle \neq \mathrm{e}^{\mathrm{i}\theta}|\phi_{\mathrm{N1}}(\mathrm{t})\rangle$. Then, generally, the electron spin and nuclear spin are entangled, and the absolute magnitude of the matrix element $|\langle\phi_{\mathrm{N0}}(\mathrm{t})|\phi_{\mathrm{N1}}(\mathrm{t})\rangle| < 1$. This case is sometimes

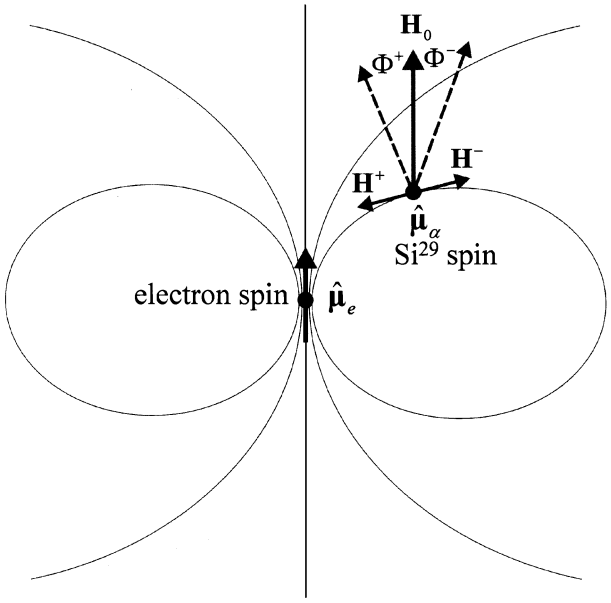


**Fig. 4.** The hyperfine interaction permits a $Si^{29}$ nuclear spin to sense an electron spin orientation through the electron's classical dipolar effective fields $\mathbf{H}_{\pm}$ tilted from the applied dc field $\mathbf{H}_0$. The $Si^{29}$ nuclear spin precesses around the axis $\Phi^+$ or $\Phi^-$ performing, in effect, a weak quantum measurement of the electron spin.

neglected in decoherence models that invoke only the dephasing term, Case 1.

The entanglement mechanism, Case 2, leads to additional nonexponential coherence decay at early times. In effect the $Si^{29}$ nuclear spins can sense the electron qubit direction. In doing so, they become entangled, and they cause decoherence.

The overall interaction between electron and nuclear spin, includes both a contact hyperfine term, as well as a classical dipole–dipole hyperfine term

$$\bar{\mu}_{\mathrm{e}} \cdot \bar{\mu}_{\mathrm{n}} \frac{8\pi}{3} |\Psi(\mathrm{r_n})|^2 + \left\langle \Psi \left| \frac{3(\bar{\mu}_{\mathrm{e}} \cdot \hat{\mathrm{r}})(\bar{\mu}_{\mathrm{n}} \cdot \hat{\mathrm{r}}) - \bar{\mu}_{\mathrm{e}} \cdot \bar{\mu}_{\mathrm{n}}}{\mathrm{r}^3} \right| \Psi \right\rangle .$$

In the presence of a dc magnetic field in the $z$ direction, sometimes only Case 1 is considered, but we will need to consider Case 2 as well. It is noteworthy that in the classical dipole–dipole coupling, the electron spin produces a dc component of transverse magnetic field at the site of the $Si^{29}$ nucleus, as shown in Fig. 4. The effective steady magnetic field B seen by the $Si^{29}$ nucleus shifts by $\Phi^+$ or $\Phi^-$ depending on whether the electron spin is up or down. This causes a difference between $|\phi_{\mathrm{N0}}(\mathrm{t})\rangle$ and $|\phi_{\mathrm{N1}}(\mathrm{t})\rangle$, and a decoherence. There are also Case 1 type decoherence terms arising from the contact hyperfine interaction [18], but those are less significant at finite magnetic fields than the classical dipole–dipole hyperfine mechanism of Fig. 4.

As a result of the mechanism in Fig. 4, the nuclear spin quantization axis is slightly different, depending on whether the electron spin is up or down. The nuclear precession caused by a change from a steady state up electron qubit to a down electron qubit is illustrated in Fig. 5, where the axis of quantization is the net magnetic field for the $|0\rangle$ state of the qubit. Thus, the nuclear precession carries forbidden information about the electron spin. The way to prevent this

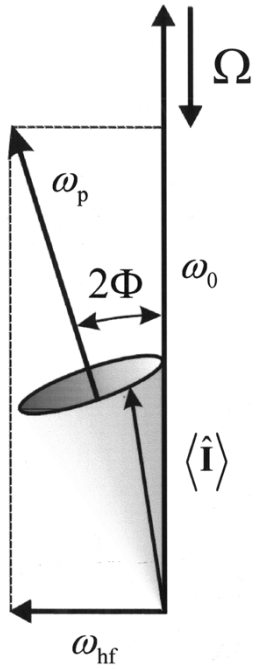


**Fig. 5.** The precession of the nuclear spin $\langle \mathrm{I} \rangle$, due to the slight tipping of the magnetic field caused by electron spin classical dipolar magnetic moment $\mu_z$. There is also a far off-resonant contribution from $\mu_{\mathrm{x}}$ and $\mu_{\mathrm{y}}$ acting through the contact hyperfine term, that are themselves precessing at a microwave frequency, $\Omega$, not shown to scale.

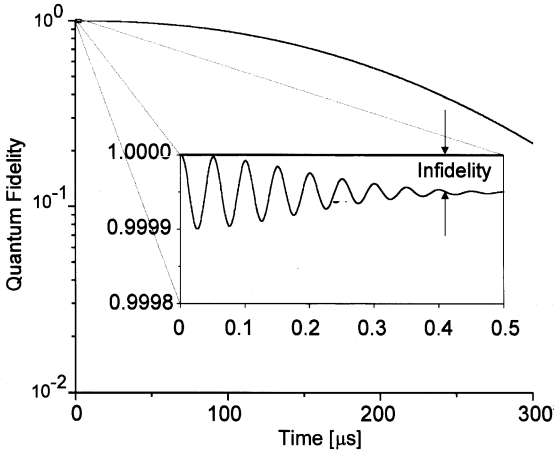


**Fig. 6.** In addition to the long time nonexponential $\exp\{-(\mathrm{t}/\mathrm{t_o})^{\gamma}\}$ decay caused by spin diffusion, there is also an initial weak ringing in the fidelity of an electron spin due to entanglement with $Si^{29}$ nuclear spins. The oscillations decay within the inverse inhomogeneous nuclear spin lifetime. An infidelity of $10^{-4}$ is already sufficient to cause concern.

problem is to have a very large dc magnetic field in the $z$ direction. Then the quantization axis becomes more rigid, and hardly moves at all with qubit flips.

The slight nuclear precession populates the inverted nuclear state. In that case, the probability of decoherence is given by the probability of an inverted nuclear population. The inset of Fig. 6 shows the slight ringing of the inverted nuclear population at the nuclear Zeeman frequency at early times. If there are many nuclei, then the all the probabilities add up to give an overall decoherence. This slight ringing in the early stages of decoherence is expected to merge

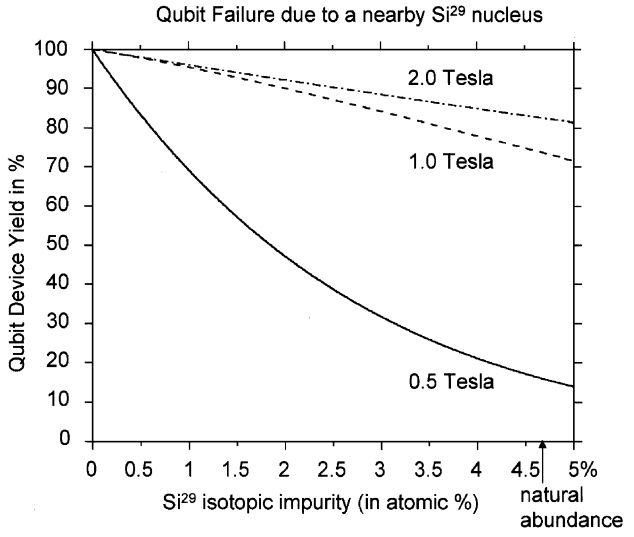


**Fig. 7.** The finite qubit yield, owing to the risk of a single nearby $Si^{29}$ nucleus in close proximity to an electron spin, contributing fidelity oscillations greater than $10^{-4}$. High dc magnetic fields are helpful in improving the device yield of qubits in which there is no entanglement at early times.

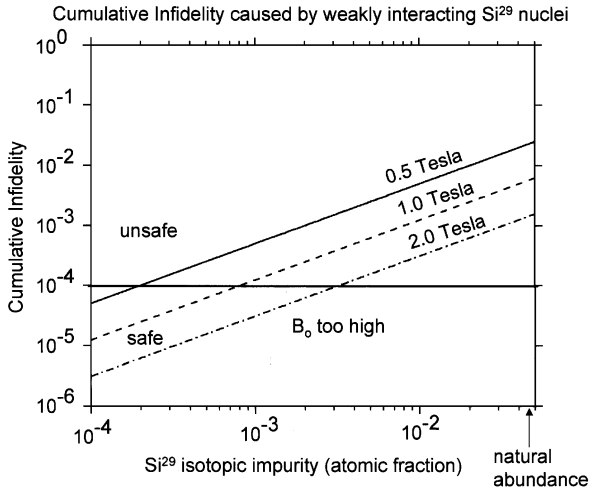


**Fig. 8.** The cumulative peak infidelity introduced by integrating up the effect of many distant $Si^{29}$ nuclei coupled weakly to the electron spin.

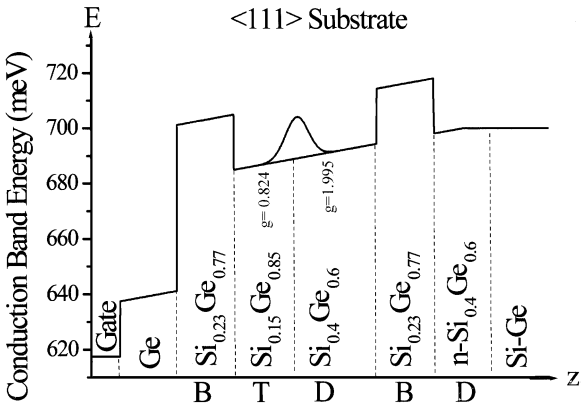


**Fig. 9.** An epitaxial layer structure of SiGe alloys, with adjacent epitaxial layers having the same conduction band energy, but different g-factors. An electrostatically confined electron wave function straddling the adjacent layers can have its g-factor manipulated by gate control.

smoothly to the slower $\exp\{-(t/t_o)^\gamma\}$ coherence decay as shown in the main part of Fig. 6. By the time the slow $\exp\{-(t/t_o)^\gamma\}$ decoherence, due to Case 1 frequency drift and phase shift effects sets in, the errors would already be too large to be correctable by quantum error correction.

For nearby nuclei, a single $Si^{29}$ can already be fatal to the electron qubit, since it could immediately sense the electron spin orientation. At finite $Si^{29}$ concentration there would only be a finite yield of good electron spin qubits. The resulting yield is plotted in Fig. 7.

In addition to the fatal effects of a nearby $Si^{29}$ nucleus, there is also the cumulative quantum error that integrates up for many distant nuclei in Fig. 8. Once again, high dc magnetic fields are helpful. The requirements of both Figs. 7 and 8 must be satisfied to minimize the initial Case 2 type errors.

It is fortunate that Silicon is 95% nuclear spin free, and that Germanium is 92% spin free. They are both subject to additional isotopic purification, that may be needed to produce a high yield of error-free spin transistors. Fig. 8 implies that an isotopic purification of 99.9% $Si^{28}$ would be valuable for a factorization engine [1] employing full error correction [16]. Isotopically pure epitaxial 99.9% $Si^{28}$ is commercially available, but we are unaware whether pure Ge isotopes are also commercially available. Such a degree of nuclear spin purification would also be useful for the recent proposal [19] that internal communication in a quantum computer should be by the direct transport of the electrons. Direct electron transport would be disturbed by a constantly changing nuclear spin environment, if nuclear spins were present.

The III–V semiconductors have *no* spin zero nuclei. This suggests that they would require an extremely high quantum-error-correction-rate to overcome hyperfine interactions, but that they could still be used for telecommunication applications. In telecom applications, quantum errors merely act to reduce the bit-rate, and errors up to 10% are reasonably tolerable.

## VII. Spin Resonance Transistor

One of the motivations for employing semiconductor spins to carry quantum information, is that such electron spin devices and systems could be made fully compatible [8] with conventional solid-state electronics. In this respect, it would be desirable to develop a transistor-like device [20] whose gate could induce single-qubit rotations in a trapped electron, and whose spin state could be read out by the source/drain current. We call such a device a *spin resonance transistor*, (SRT) to be distinguished from the *spin transistor* [21] that does not store quantum information, and whose main function is to control charge transport as in a conventional transistor.

A key guiding principle of SRTs is that the g-factor, or the Zeeman energy splitting can be controlled by an external gate voltage. Indeed, in an anisotropic band structure, the g-factor becomes a g-tensor allowing full three-dimensional electron spin control [22]. An example of such control is illustrated in Fig. 9, a cross-sectional view of strained $\langle 111\rangle$ $Si_{1-x}$ $Ge_x$ heterostructure, in which adjoining layers

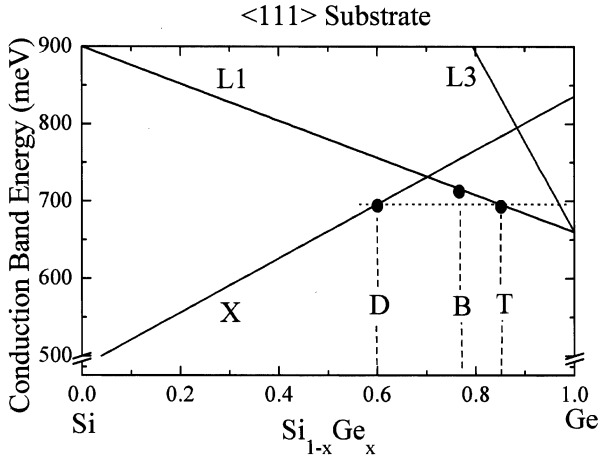


**Fig. 10.** Conduction band energy versus alloy composition for the epitaxial structure of Fig. 9. The different epitaxial layer compositions are labeled D, B, T, etc. The conduction band minima are labeled L1 and L3 for the strain split Ge-like conduction bands, and X for the Si-like conduction bands.

of different g-factor have the same conduction band energy. The corresponding conduction band energies are illustrated in Fig. 10, versus composition. The g-factor can be strongly modulated over a small compositional range near $x = 0.7$, where the conduction band minimum switches from a Si-like X-band minimum, $g = 1.99$, to Ge-like L-band minimum $g = 0.823$. If an electron is electrostatically trapped in such adjoining layers, then a gate electrode can switch the electron between the adjoining layers, modulating the g-factor, or indeed the g-tensor.

Indeed, there are a whole range of semiconductor heterostructure compositions and strains that can create a rich variety of g-factor controlled devices. Fig. 11 depicts g-factor versus [23] lattice constant for a variety of III–V semiconductor alloys. Plotted on the same horizontal axis is bandgap energy versus lattice constant, a famous graph that is of great value in optoelectronics. Among the noteworthy features of Fig. 11, are lattice matched III–V alloys that have g-factors of opposite sign. GaAs has $g = -0.44$, while $Ga_{0.7}\,Al_{0.3}\,As$ alloys have $g \approx +0.4$. Another important combination of great value in optical communications is $Ga_{0.47}\,In_{0.53}\,As$ lattice matched to InP substrates and epi-layers. $Ga_{0.47}\,In_{0.53}\,As$ has $g = -4.5$, while InP has $g = +1.2$.

Spin control is particularly powerful when the g-factor can be made to change sign, or the g-tensor components can be manipulated in both sign and magnitude. An electrostatic gate electrode can then induce any type of desired spin rotation. We will show below, that quantum information can be transferred from a photon polarization to an electron spin polarization. Band structure engineering, i.e., quantum confinement, strain, and alloy composition, can assure that the required selection rules are obeyed, and that the g-factors are engineered [24] to have the right magnitude and sign.

Given that the g-factor can be modulated electro-statically, it can be tuned in and out of electron spin resonance causing spin flips. A number of experiments [25], [26] have now demonstrated gate controlled spin flips in transistor-like structures. An example of such a transistor structure is the

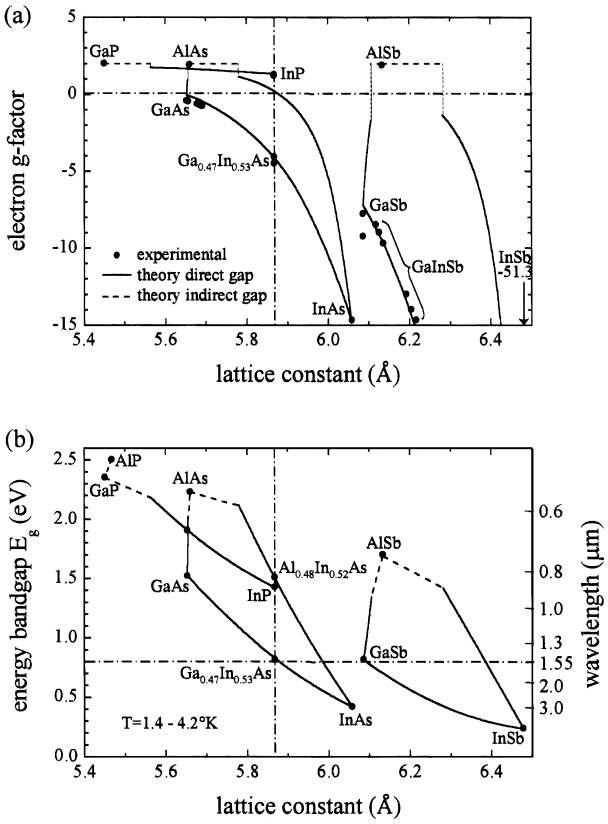


**Fig. 11.** (a) A global survey of published III–V g-factors versus lattice constant. (b) The corresponding graph of bandgap versus lattice constant that is a famous in optoelectronics. The horizontal and vertical lines inside the graph indicate respectively, the optimum wavelength for optical fiber telecommunications, and the lattice constant of InP, the substrate of choice for telecommunications devices.

$Ga_{0.7}\,Al_{0.3}As$– GaAs two-dimensional (2-D) electron gas (2DEG) heterostructure is shown in Fig. 12. The gate shifts the wave function of the electrons in the 2DEG.

The electrical test setup as shown in Fig. 13 resembles a conventional field effect transistor, (FET), except that it is bathed in microwaves to induce spin-flip transitions. The method of detecting spin flips is by the change in magneto-resistance in the source/drain channel, that is particularly sensitive [27] at odd filling factors in the quantum Hall effect. The gate manipulates the spin orientation through electron spin resonance, while the source/drain channel resistance monitors the spin flips. A resistance change of about 10 Ω out of 230 Ω is produced by spin flips at the resonance condition. The g-factor tuning is demonstrated [25] in Fig. 14, by both a front gate, and a back gate, with tuning in opposite directions of g, verifying the tuning model in Fig. 12. A broader tuning range all the way to a sign reversal of g-factor, was demonstrated by Salis *et al.* [26] using optical detection.

The demonstration in [25] would nearly achieve our ideal for SRTs, except that, millions of electrons were needed to produce the desired signal. It will be necessary to electrically detect a single quantum state of a single electron spin, to fully demonstrate a SRT. That would require a potential trap for a single electron adjacent to an FET channel. The spin orientation would have to be converted to an electric charge by

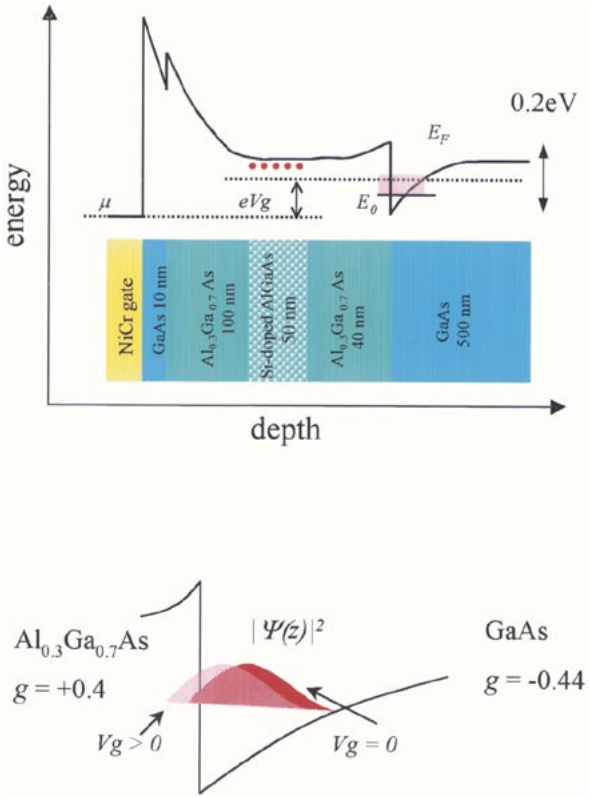


**Fig. 12.** (a) Schematic diagram of the conduction band of the modulation doped GaAs– $Al_{0.3}$ $Ga_{0.7}$ As heterostructure. Fermi level, $E_F$, the chemical potential, $\mu$, and the lowest energy level of the quantum well (QW), $E_0$, are indicated. (b) The 2-D electrons are trapped in the "triangle"-shaped QW near the interface between the GaAs and $Al_{0.3}$ $Ga_{0.7}$ As materials. The electron wave function shifts back and forth for bias voltage $\mathrm{V_g} = 0$ and $\mathrm{V_g} > 0$ between $\mathrm{g} = -0.44$ and $\mathrm{g} = +0.4$.

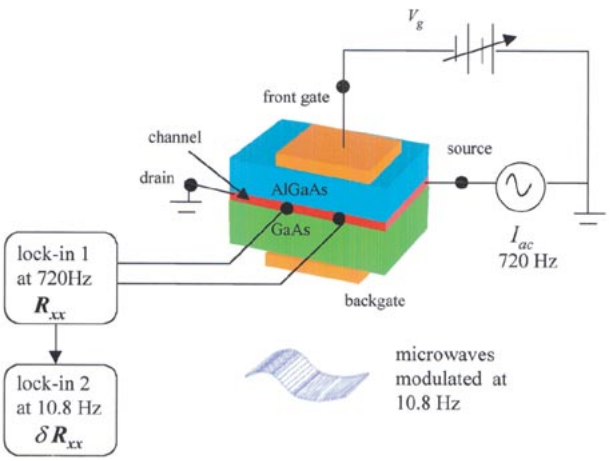


**Fig. 13.** Schematic diagram of the experimental setup for a SRT where the gate controls the electron spin resonance frequency, and the source/drain channel resistance monitors the spin orientation.

means of spin-dependent tunneling[2] [28] or singlet state [8] formation. FETs easily have single electric charge sensitivity.

Single spins have been detected optically, [29] and [30], by multiple luminescence cycling through a triplet state, but that

[2]There have also been intriguing scanning tunneling microscope results by C. Durkan and M. E. Welland, but these are also ensemble-type measurements.

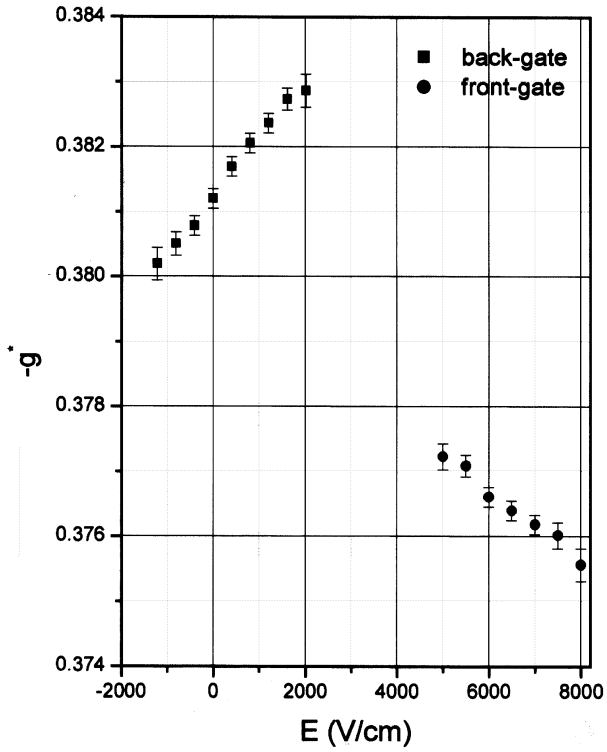


**Fig. 14.** The g-factor of the electrons in the AlGaAs–GaAs 2DEG, acting as a source drain channel, as tuned by a front gate or a back gate. The direction of tuning is opposite in the two cases.

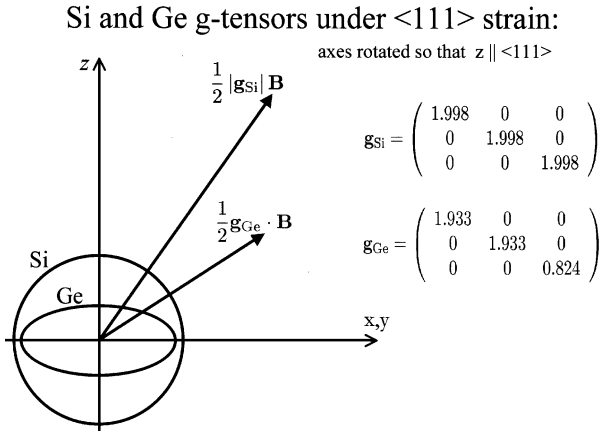


**Fig. 15.** The g-tensor ellipsoid for electron spins in Si-rich alloys, and in Ge-rich alloys. For Si-rich alloys g is near two, and practically isotropic. For Ge-rich alloys, the anisotropic g-tensor can be manipulated to control the motion of the spin.

is ultimately an ensemble measurement since it needs to be repeated thousands of times to achieve [31] single spin sensitivity. Most recently Wrachtrup has demonstrated optical spectral resolution of a single magnetic sublevel [32] of the NV center in diamond by the same technique. This may be the first detection of a single spin state in condensed matter. Electrical detection of a single spin state will be the critical milestone for the creation of the SRT.

In this section, we have shown that the SRT could be used for single-qubit rotations. It also appears likely that the milestone of single spin state detection in such a transistor-like device will be reached soon. If these capabilities were also

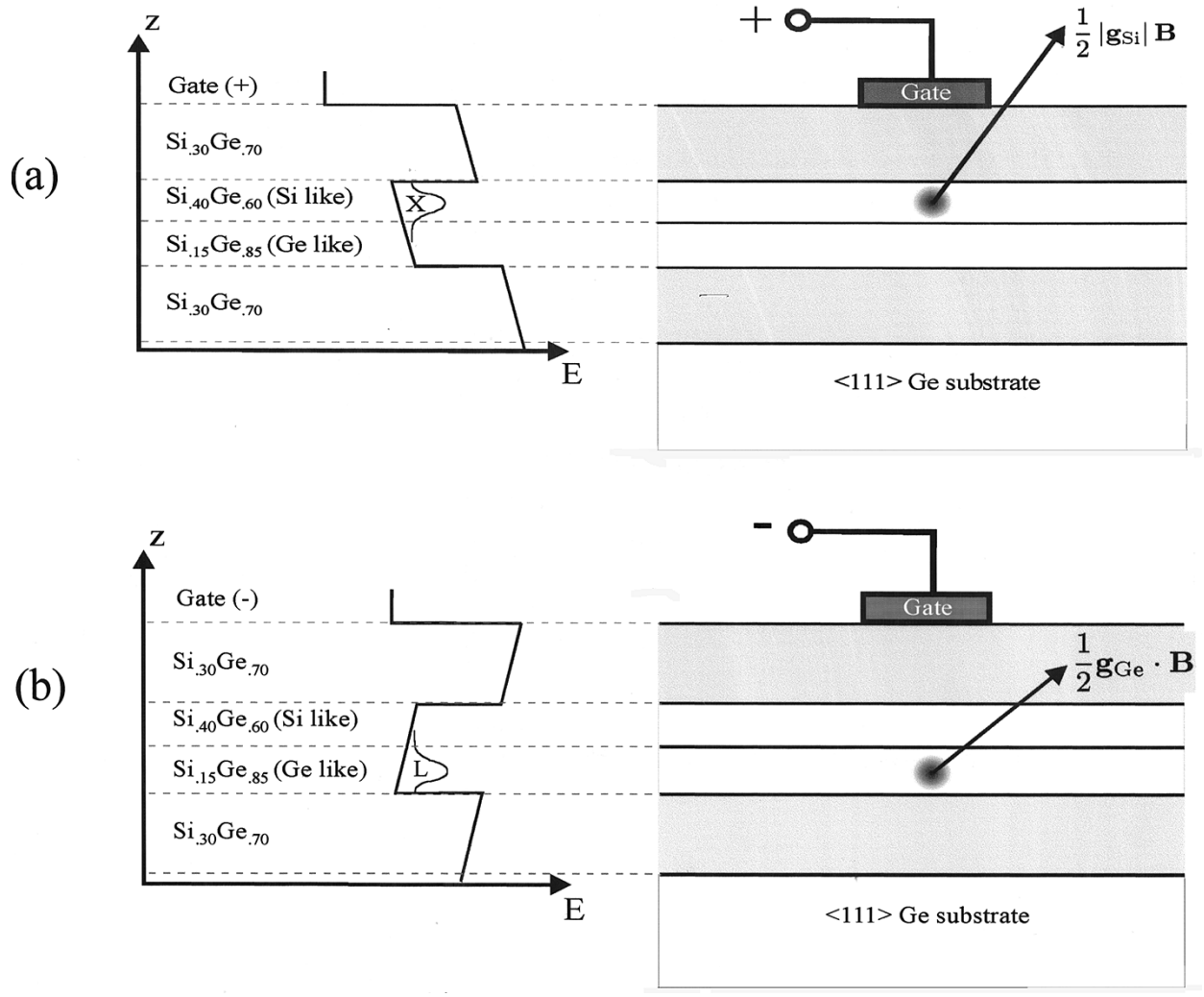


**Fig. 16.** As the electron is shifted electrostatically between (a) the X-minimum (Si-like) and (b) the L-minimum (Ge-like), the effective direction of the magnetic field can change by up to 20° owing to the anisotropic g-tensor properties.

augmented by the gate induced exchange interaction [33], then the three major functions for quantum computation would be met: single-qubit logic gates, double-qubit logic gates, and spin state readout.

## VIII. g-Tensor Modulation in Spin Resonance Transistors

In an anisotropic band structure, the g-factor becomes a g-tensor allowing single-qubit rotations [22], and spin resonance [34] without a microwave magnetic field. A microwave field of $\sim$ 450 kW/cm$^2$ would be required to produce an electron spin rotation in a quantum logic clock period of 1 ns. Such high microwave power densities are generally impractical, and incompatible with cryogenic temperatures. To solve this problem, there have been a number of suggestions that would permit universal quantum computation, without requiring single-qubit rotations. For example DiVincenzo *et al.* [35] have proposed an all-inclusive quantum logic that requires only the exchange interaction. However that scheme requires three times the number of spins, and ten times the number of exchange gate operations.

The key to eliminating the microwaves is to recognize that the g-factor is actually a g-tensor. Then the Hamiltonian can be written $\mu_{\mathrm{B}}\,\vec{\mathrm{S}}\cdot\overleftrightarrow{\mathrm{g}}\cdot\vec{\mathrm{B}}$, where $\mu_{\mathrm{B}}$ is the Bohr magneton, S is the spin vector, B is the magnetic field vector, and g is a tensor as illustrated in Fig. 15. The g-tensor for electrons in Silicon rich alloys is almost isotropic, but Ge rich alloys, owing to their characteristic conduction band minima, have a rather anisotropic g-tensor, with a much lower $\mathrm{g}_{zz} \approx 0.824$ component. If $\overleftrightarrow{\mathrm{g}}\cdot\vec{\mathrm{B}}$ were to be regarded as an effective magnetic field vector, $\vec{\mathrm{B}}_{\mathrm{eff}} \sim (1/2)\overleftrightarrow{\mathrm{g}}\cdot\vec{\mathrm{B}}$, then the *direction* of the effective magnetic vector could be modulated in a SRT, similar to the one in Fig. 9. (The normalization factor 1/2 guarantees that $\mathrm{B}_{\mathrm{eff}} = \mathrm{B}$ for a free electron $\mathrm{g} = 2$)

Such $\mathrm{B}_{\mathrm{eff}}$ directional modulation can be created by the gate electrostatic field moving the electron between Ge-rich and Si-rich epitaxial layers, producing *directional* modulation of the $\vec{\mathrm{B}}_{\mathrm{eff}}$ vector as illustrated in Fig. 16. The $\mathrm{B}_{\mathrm{eff}}$ vector can be regarded as being digitally modulated between the two extreme limits of the Ge-rich and Si-rich alloys corresponding respectively to electrons that are either L-like or X-like. At the modulation limits the g-tensor is compositionally fixed, and relatively independent of gate voltage. That

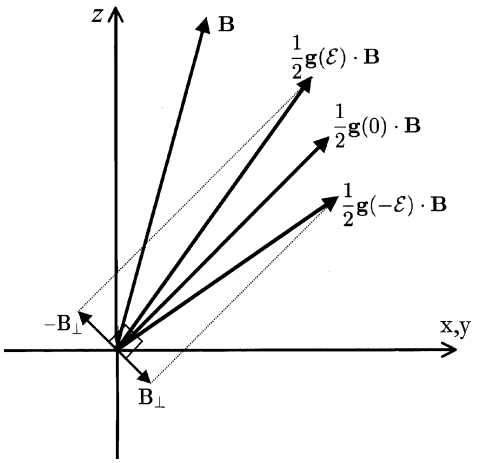


**Fig. 17.** The electrostatic directional modulation of the effective magnetic field $B_{eff}$ through the anisotropic g-tensor, produces a similar electron spin resonance as a huge transverse microwave field $B_\perp$. A few ac cycles are sufficient for a rotation of electron spin to an arbitrary point on the Bloch sphere.

should lead to robust and accurate gate operations. Using the numerical values of the Si–Ge g-tensors, about 20° of angular modulation is available at the limits. A few cycles of alternating the g-tensor back and forth, for half-precession periods, would suffice to orient the electron spin to any chosen point on the Bloch sphere.

This spin rotation can also be thought of as a form of conventional magnetic resonance in which there is a transverse oscillating magnetic field, added vectorially to the large dc magnetic field. That interpretation is illustrated in Fig. 17, with oscillating transverse effective magnetic field caused by the alternating sign of the gate electric field $\mathcal{E}$. A specially pulsed radio frequency (RF) waveform on the gate comprising only ~1 pico-Joule, can produce the desired single-qubit rotations in ~1 ns.

The combination of robust single-qubit operations, with only a few RF cycles of gate signal, makes g-tensor modulation the preferred operating mode of SRTs.

## IX. Entanglement Preserving Photodetectors

Individual photons are an ideal medium for the telecommunication of quantum information. The basic quantum logic functions, together with spin state readout, must be augmented by an interface to photons. Fortunately there has been great progress in the optoelectronics of single photons in the past few years.

While single photon detectors of high quantum efficiency have been known for a long time (e.g., avalanche photodiodes), single-photon light-emitting-diodes have just begun to emerge. Early models of single photon emitters were based on the Coulomb Blockade [36] of electrons on a small island. More recent versions resolve the Coulomb spectral shift of multiple excitons on a small quantum dot, followed by spectral selection [13] of single exciton emission. These types of one photon sources and detectors support quantum cryptography [37], and postselection-based linear optics quantum computing [12] (LOQC) as well.

In addition to single photon emitters and detectors, quantum repeaters also require storage of quantum information. In this regard it has already been shown that electrons trapped in semiconductors can store coherent [15] spin information. If we could transfer photon polarization directly to electron spin polarization, it would allow storage, but it would also allow quantum logic gates similar to the SRT. (Several proposals already exist to transfer quantum information from photons to atoms trapped in high-Q optical cavities [38].)

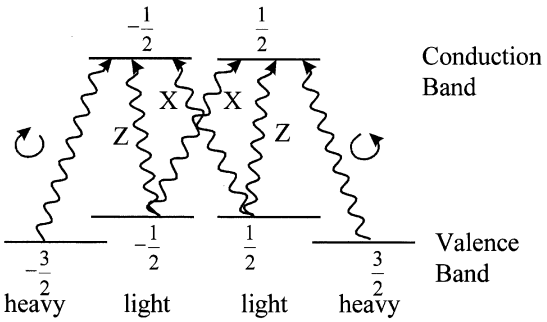


**Fig. 18.** The valence and conduction band energy levels in a typical $\langle 001\rangle$-strained III–V semiconductor showing the individual magnetic sublevels, including the light and heavy holes. Certain of the allowed optical transitions are indicated for circular polarization, and for linear polarization in the X and Z directions. (Z is the quantization axis, and the wave vector can be in any direction compatible with the optical polarization).

It is well known that polarized electrons can be created by illuminating GaAs with circularly polarized light. The valence band of GaAs has orbital angular momentum $\mathrm{L} = 1$. When combined with the spin of the electron $\mathrm{S} = 1/2$, this gives rise to four $\mathrm{J} = \mathrm{L} + \mathrm{S} = 3/2$ states. The conduction band wave function is an S-wave, with $\mathrm{J} = 1/2$. Some of the selection rules are illustrated in Fig. 18, where optical polarization is indicated by the cartesian symbols, X, Z, and the circular polarization arrows with respect to a $\langle 001\rangle$-strained III–V semiconductor. (Z is the quantization axis, and the wave vector can be in any direction compatible with the optical polarization.) A right-handed circularly ($|\mathrm{m_j}| = 1$) polarized photon, couples the heavy valence band with $\mathrm{m_j} = -3/2$ only to the conduction band $\mathrm{m_j} = -1/2$ state. Thus, upon irradiation with right-handed circularly polarized light, only electrons with spin down are created. Similarly, left-handed circularly polarized light only creates spin up electrons. This polarization sensitivity is in fact used in photocathodes for spin polarized high-energy electron accelerators.

Nonetheless, this system is not suited for transferring quantum information, encoded in an arbitrary superposition of polarization states, from a photon to an electron. Consider a photon qubit, in a superposition of circular polarization states

$$|\phi\rangle_{ph} = \alpha|\sigma^+\rangle + \beta|\sigma^-\rangle. \tag{1}$$

Since the two polarizations couple two different valence band states to the respective conduction band states, they will also create two different hole states. The electron, thus, created will be entangled with the hole, with the final state of the electron-hole pair given by

$$|\psi\rangle_{eh} = \alpha\left|\mathrm{m_j}=-\frac{3}{2}\right\rangle_h\left|\mathrm{m_j}=-\frac{1}{2}\right\rangle_e + \beta\left|\mathrm{m_j}=\frac{3}{2}\right\rangle_h\left|\mathrm{m_j}=\frac{1}{2}\right\rangle_e. \tag{2}$$

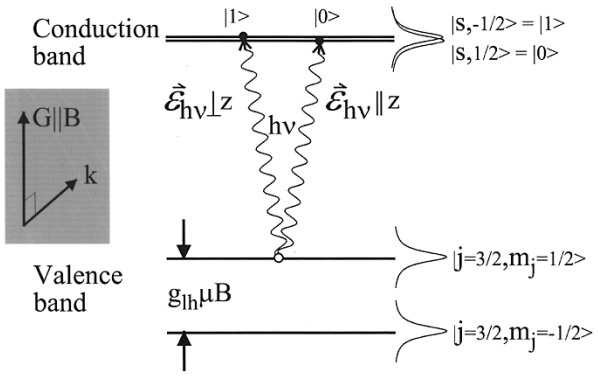


**Fig. 19.** A possible configuration for an entanglement preserving photodetector, that transfers photon polarization to electron spin polarization. The k-vector of the incident light is perpendicular to the sample normal and magnetic field, $\mathrm{k} \perp \mathrm{G}\|\mathrm{B}$. The optical electric field $\mathcal{E}$ induces transitions to either of the electron spin states, depending on its own polarization. The spin states are energetically separated by a static magnetic field. Horizontally polarized photons have an electric field perpendicular to the static magnetic field, and excite only $\mathrm{m}_s = -1/2$ conduction band electrons. The electric field of vertically polarized photons is parallel to the static magnetic field, and excites only orthogonal $\mathrm{m}_s = 1/2$ electrons. A single magnetic sublevel in the valence band needs to be spectrally resolved, requiring a large light hole $g_{\mathrm{lh}}$-factor, but the electron spin states should be indistinguishable and have a small $g_{\mathrm{e}}$-factor.

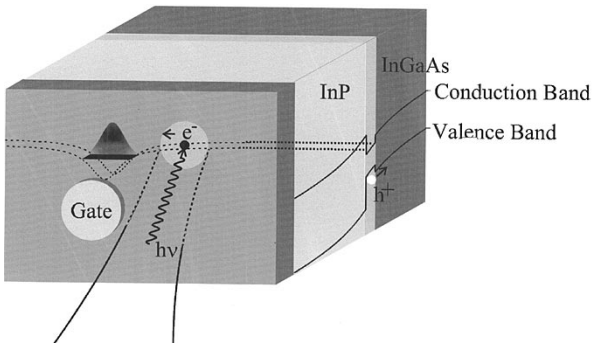


**Fig. 20.** A pictorial diagram of an entanglement preserving photodetector. The photo-hole carries no quantum information and is swept away, while the photo-electron quickly diffuses to a trap under a gate electrode on a time scale short compared with $\mathrm{T}_2$ dephasing times.

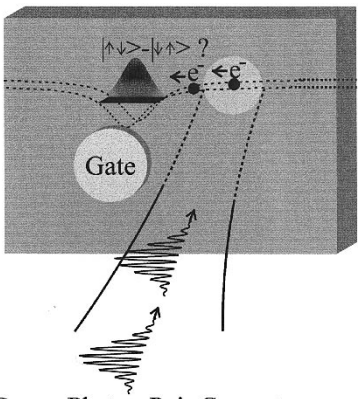


**Fig. 21.** Demonstration of entanglement preservation in the photodetector of Fig. 20. If an entangled pair of photons are derived from a parametric down converter and absorbed in the photodetector, the transfer of entanglement to their two photo-electrons can be monitored by trapping them in a shallow potential well that binds singlet pairs. A shallow well cannot trap spin triplets.

This is an undesirable state, since in order to preserve the quantum information, or process it, we would have to maintain coherence for both the electron and the hole. Most likely the hole would interact with the rest of the system and the superposition would collapse into one of the two system eigenstates in (2), and destroy the quantum information.

To avoid this problem, we have to make sure that no information is left behind in the hole state. Therefore, the two conduction band polarizations have to be accessed from a single common valence band state. The two orthogonal photon polarizations should couple the single valence state to both conduction band electron spin states. Among other requirements, this relies on the capability to create a completely nondegenerate light-hole valence band state, as shown in Fig. 19.

The topmost valence band can be optically selected by using photons that barely span the bandgap. The other valence bands would be too far below the valence band edge, and not energetically accessible. The degeneracy between heavy hole states $(\mathrm{m_j} = \pm 3/2)$ and light hole states $(\mathrm{m_j} = \pm 1/2)$ is lifted if the semiconductor is under strain, by growing heterostructures of materials with different lattice constants. Generally, in compressively strained semiconductors, the heavy hole band is the topmost band, while semiconductors under tensile strain have the light hole band on top. The growth direction G, thus, establishes a quantization axis. Finally, the remaining degeneracy between the spin up and spin down components of both bands is lifted by a static magnetic field. The proper hierarchy is strain splitting, should be greater than Zeeman splitting, which should be greater than the optical linewidth.

A detailed discussion of the selection rules—under alternative relative directions of, the magnetic field $\vec{\mathrm{B}}$, the growth axis $\vec{\mathrm{G}}$, light propagation direction $\vec{\mathrm{k}}$, and optical polarization vector E—is given in the paper by Vrijen [39] *et al.*. The net result is that both electron spin polarizations are simultaneously accessible, but need not be entangled with any other internal degrees of freedom in the semiconductor.

An illustration of such a photodetector, that would trap and store the electron spin in a potential well, is shown in Fig. 20. The electron is absorbed in a tensile strained QW, and then trapped for spin storage at an electric potential minimum created by external electrodes. The optimal band structure engineering of the QW, including its strain, thickness, and composition has been analyzed in a series of papers by Kiselev [24] *et al.*

To the degree that the trapped electron spin maintains its spin coherence, it can also maintain and preserve its prior entanglement with other quantum systems. For example, the photo-electron may have originally been derived from a photon that was one member of a parametric down-conversion pair, or one member of a singlet pair. The correspondingly produced photo-electrons should also maintain that entanglement. A schematic diagram of such an experiment is in Fig. 21, that illustrates the creation of a photo-electron singlet pair from the corresponding parametric down-converted photons. Thus, the name: "entanglement preserving photodetectors."

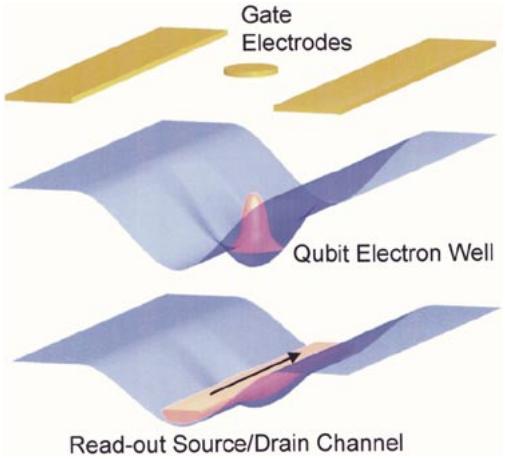


**Fig. 22.** A conceptual diagram of the general SRT concept, with gate electrodes forming both a qubit trap, and an adjacent source/drain readout channel. Single electric charges are sufficient to influence the source/drain resistance. Tunneling between a spin polarized channel and the qubit well can be used for spin readout.

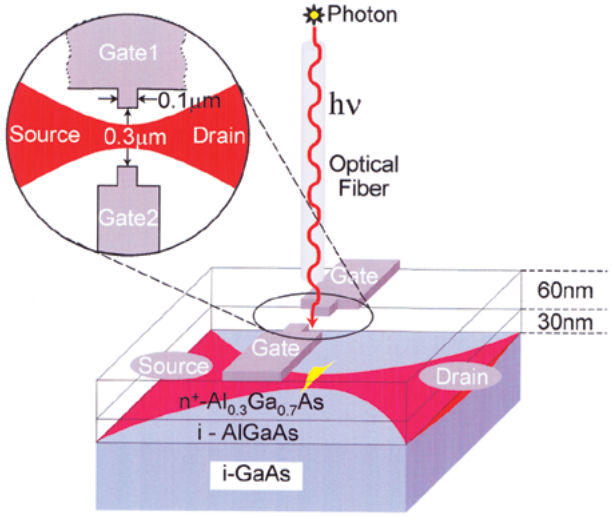


**Fig. 23.** An implementation of the trap and readout channel concept for the detection of single photons, and single photo-holes. A 2DEG is pinched off into a narrow source/drain channel whose resistance is very sensitive to single electric charges.

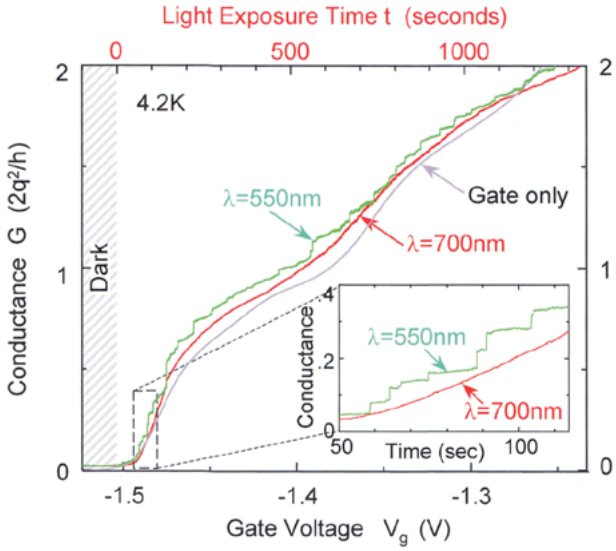


**Fig. 24.** The source/drain channel conductance induced by a positive modulation of the gate voltage, and equivalently by a timed light exposure, that has the same effect as gate voltage. In the AlGaAs–GaAs material system, the light exposure produces trapped photo-holes that increase the channel conductivity. The conductance quantization plateaus at multiples of $2e^2/h$ are practically identical for photo-holes, and for positive gate voltage only. With light at $\lambda = 550$ nm, there is the additional feature of individual small conductance steps associated with single photons.

## X. Detecting Single Photons and Measuring Single Qubits

There are a number of amplification processes that make it possible to detect single photons or single electrons. Most common is avalanche multiplication, in a Silicon photo-diode, or in a photo-multiplier. Avalanche multiplication is a rather violent process that unfortunately does *not* preserve quantum information.

There is another gain mechanism, sometimes called photo-conductive [40] gain, that is much more gentle. This is a photo-conductive process in which a photo-electron is trapped, and then its electrostatic repulsion influences the electrical conductivity of a channel. The gain arises because one trapped electron can influence the conductivity of millions of electrons passing through a channel. The channel can be the source/drain channel of a transistor, while the photo-electron trap can be a positively charged donor ion, or a potential well formed by gates, or some other type of trap.

Equally well, such an electron trap can hold a qubit, and its spin can be measured by the technique of spin/charge conversion proposed by Kane [8]. Spin/charge conversion operates by

1) spin-dependent tunneling [28], a transition from charge 1 to charge 0; or
2) singlet pair formation [8], a transition between charge 1 to charge 2.

Fig. 22 shows the general SRT concept, with the electron trap formed by electrostatic gates, and below it a source/drain channel whose resistance will be substantially influenced by a trapped electric charge. Tunneling would operate from the electrons in the channel, to/from the potential well. Such tunneling events are commonly observed [41] in low-temperature transistors, where they give rise to the so-called "random telegraph signal." These are fluctuations in resistance caused by the charging and discharging of a long-lived trap.

Near pinch-off, a source/drain channel will have a resistance of order $\hbar/q^2 \approx 26\ \mathrm{k}\Omega$, but a single electric charge q near the channel can modify the resistance by almost that amount. Thus, when a transistor is in the random telegraph mode, it is acutely sensitive to single electron charges. An electron trapped in a semiconductor potential well remains in a rather benign environment, in which spin entanglement information may be preserved. Accordingly, the first step is to use the photoconductive gain mechanism for single electron detection.

A practical device structure implementing the trap and channel concept of Fig. 22 is shown in Fig. 23. Electrostatic gates pinch off a source/drain channel in an AlGaAs–GaAs 2DEG. Photo-holes are trapped at neutral donors, or in

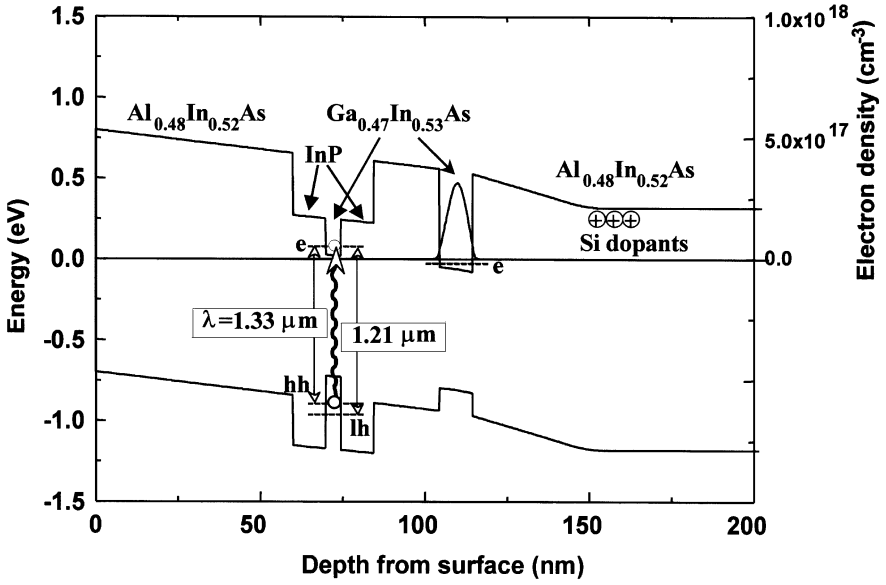


**Fig. 25.** The energy band diagram of the single photoelectron detector at zero bias simulated by the one-dimensional Poisson/Schrödinger equation. There is a modulation doped channel at a 110-nm depth, and an undoped channel at about 70-nm depth. Photo-induced transitions between the heavy hole band and the conduction band are shown with an arrow. Photo-ionization of neutral donors by $\lambda = 1.77$-$\mu$m light effectively modulation dopes the channel. The tunnel leakage time between the two QWs is estimated to be over 1 h by WKB simulation.

DX-centers near the channel. The individual carrier trapping events each produce a step in source/drain current as shown in Fig. 24. The fact that the photo-conductivity is of the normal, positive kind, indicates that photo-holes rather than photo-electrons are being trapped in Fig. 23. Light of wavelength $\lambda = 550$ nm is strongly absorbed, and produces carriers very near the channel allowing single charge sensitivity, as indicated by the individual conductance steps. Light at $\lambda = 700$ nm is absorbed more deeply in the semiconductor producing a general increase in source/drain current, but without the individual photon steps being resolved. This photo-hole trapping experiment is more thoroughly discussed in [42].

While the trapping and detection of individual photo-holes represents a new type of single photon detector, holes are not generally desirable for storing quantum information. Owing to the hole's $l = 1$ orbital motion, they are expected to have short spin dephasing times. The presence of negative DX- centers in the AlGaAs alloys, means that hole-trapping will dominate over electron trapping. Indeed, the signature of electron trapping, negative persistent optical photo-conductivity has never been observed. Accordingly we have introduced InAlAs–InGaAs–InP alloy systems, (where the DX-center does not form), for trapping electrons.

The type of heterostructure that we use for electron trapping [43] is illustrated in Fig. 25. At a depth of 70 nm, there is an undoped $Ga_{0.47}In_{0.53}As$ QW with a bandgap at $\lambda = 1.33$ $\mu$m. This is the region where we hope to trap electrons. At a depth of 110 nm there is another $Ga_{0.47}$ $In_{0.53}$ As QW, this one modulation doped, that can act as a source/drain channel to sense trapped electric charges. The modulation doping comes from a buried $n - Al_{0.48}$ $In_{0.52}$ As layer, Si-doped. The barriers in this structure are $Al_{0.48}$ $In_{0.52}$ As rather than InP to take advantage of the higher conduction band barriers in the Aluminum alloy.

The top and side views of the photodetector are illustrated in Fig. 26(a) and (b). Negatively biased gate electrodes are shaped to pinch off a channel in the modulation-doped layer, while creating a parabolic potential under the relatively positive central circular region. This gate geometry was designed to trap individual electrons in the parabolic well in the undoped layer, as illustrated in Fig. 26(b). While we do see evidence of electron trapping, it is not clear whether the electrons are being trapped at the parabolic potential well or at ionized donors. Fig. 26(c) and (d) shows scanning electron micrographs (SEMs) of the gate structure.

Long wavelengths $\lambda > 1.33$ $\mu$m produce a positive persistent photoconductivity, as indicated by the $\lambda = 1.7$ $\mu$m curve in Fig. 27, presumably due to photo-ionization of neutral donors. This can be used to adjust the modulation doping density and pinchoff voltage as illustrated in the inset to Fig. 27. If the initial "light bias" and voltage bias do not completely pinch off the channel, then $\lambda = 1.3$ $\mu$m light produces a negative persistent photoconductivity in Fig. 27. But now, the photon induced conduction steps are negative, indicating electron storage. We believe this is the first [43] observation of negative persistent photoconductivity, and the first [43] observation of negative photon steps in photoconductivity.

Light of wavelength $\lambda \sim 1.3$ $\mu$m falls in the intermediate range, sometimes producing a conduction band electron in the channel to be trapped, or sometimes causing photo-destruction of the trapped electron, both depending on the initial bias condition. Fig. 28 illustrates the random telegraph signal from the trapping and detrapping of an electron. The trapping and detrapping events are induced by light during the consecutive 10-s open-shutter-periods or pulses, labeled

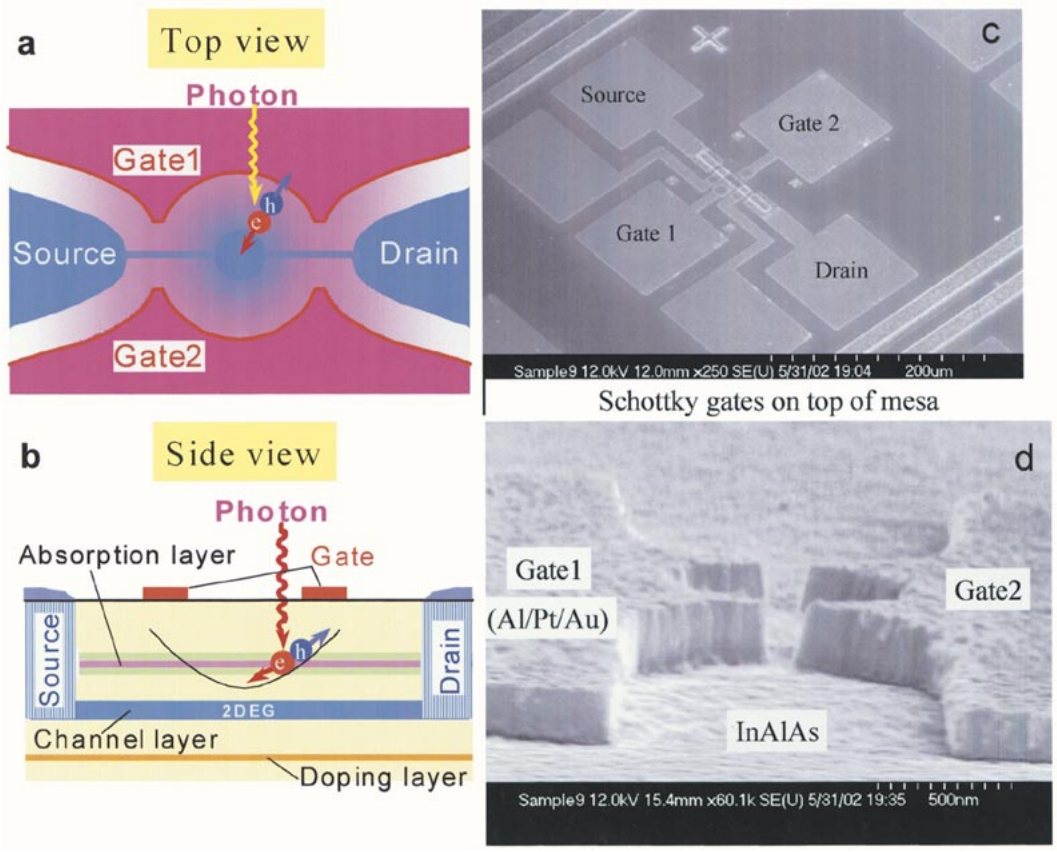


**Fig. 26.** A single photoelectron detector with a window-gate double-quantum-well modulation-doped heterostructure. (a), Top view of the window-gate design. The center of the window gates is relatively positive to the surroundings when negative voltage is applied to the gates because of Fermi level pinning. The central blue regions indicate the shape of the 2DEG in the channel layer. (b) Cross-section view of the layers. The upper QW functions as an absorption layer and lower QW serves as a 2 DEG channel layer, which is connected to source and drain. The curve on the absorption layer illustrates the parabolic electron potential when negative voltage is applied to the gates. (c) SEM picture of the single photo-electron detector. (d) Close-up perspective SEM picture of the metallic window gates on the top of the semiconductor. The window diameter is 1 $\mu$m.

a, b, c, . . . etc. The 10-s open-shutter pulses repeat every 50 s, allowing about 30 photons to fall on the detector area during each period.

Successive optical pulses usually produced either electron trapping or photo-ionization, alternating, depending on the previous state. Sometimes multiple optical pulses were required before the state would alternate in Fig. 28. Within the 10-s optical pulse there might be a transient thermal response, especially in time slot g; but that returned to either of the two alternating states after the optical pulse. Thus, we have observed optically induced trapping and detrapping of individual photo-electrons. In principle, their spin could be measured by either of the spin-to-charge transformation mechanisms; spin-dependent tunneling or singlet state formation. Depending on the decoherence lifetime of the trapped electron spin, these could be quite useful for storing and manipulating quantum information.

## XI. Design of an Optoelectronic Quantum Repeater

While the implementation of a Quantum Factorization engine would require the control of thousands of qubits, a quantum repeater implementing the algorithm of Fig. 1 requires only three qubits. Thus, a quantum repeater could be an important transitional stage to more complex quantum information circuits later on.

An optical quantum repeater has its own complexities however. A photodetector and light emitter would have to be directly integrated together with qubit storage and processing. Such direct integration is needed because our ability to transport qubits is quite limited. A moving electron spin qubit is quite susceptible to decoherence, since it sees a constantly changing nuclear spin environment. Short distance transport by drift or diffusion is acceptable however. A side view of our proposed integrated optoelectronic quantum repeater is shown in Fig. 29.

The need for closely spaced integration presents immediate difficulties. Both the photodetector and the light emitter need to be made of direct bandgap III–V semiconductors, for efficient performance. During the quantum repeater algorithm, long-term spin storage is required, for at least a round-trip time to the next repeater station. Such storage is best implemented in an isotopically purified group IV semiconductor. Thus, the "front end," the photodetector and light emitter need to be III–V, while the storage and quantum logic

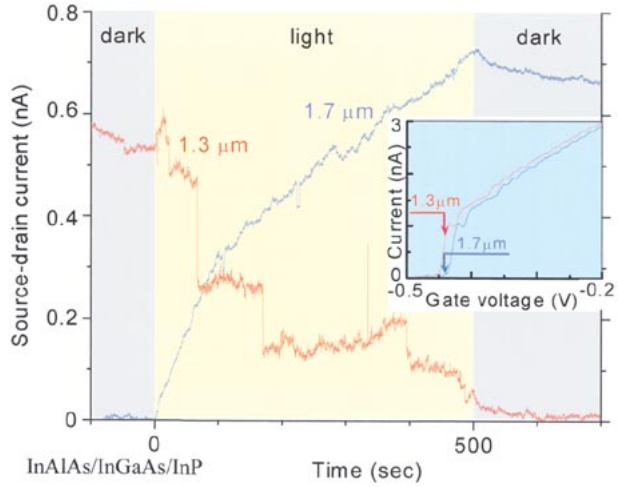


**Fig. 27.** Negative persistent photoconductivity of the single photo-electron detector due to $\lambda = 1.3\ \mu$m light starting with finite conductance, and positive photoconductivity at $\lambda = 1.7\ \mu$m light starting with zero conductance. The source-drain current drops in discrete steps when the detector is exposed to $\lambda = 1.3\ \mu$m. (The inset shows the initial current-gate voltage characteristics, $I_{sd} - V_g$ curves, controlled by soaking the sample in $\lambda = 1.7\ \mu$m light.) The $\lambda = 1.3\ \mu$m photons create photoelectrons in the QW, which are trapped and pinch off the 2 DEG, step by step. In contrast, the $\lambda = 1.7\ \mu$m photons photoionize the neutral donors and increase the 2 DEG density. Photon number absorbed in the window area is 0.3/s, on average.

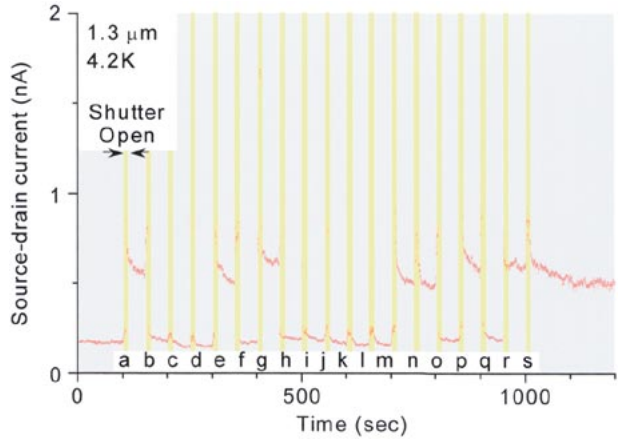


**Fig. 28.** Bit-wise current state switching near the cross-over from positive to negative photoconductivity. The photon source is gated, to help synchronize the current steps with the photons. The shutter was repeatedly opened for ~10 s every 50 s. The negative and positive photoconductivity events (electron trapping and photo-neutralization), were initially brought into near balance by adjusting the electrostatic configuration by using light soaking at $\lambda = 1.77\ \mu$m to adjust the modulation doping. The current alternates between a higher state and a lower state, the switching induced by optical pulses. In the dark, the state was stable for more than 1 h. The photon number absorbed within the window area is 30 photons in 10 s, on average.

need to be in a group IV semiconductor. Can we safely transport a spin across the interface between a III–V and Silicon?

An affirmative answer is suggested by the demonstration by Awschalom and colleagues of successful [44] spin transfer across the ZnSe–GaAs hetero-interface. This demonstrates again, if it was needed, that electron spin is a rather robust degree of freedom. Wafer fusion has been successfully applied to the formation of InP–Si heterojunctions, across which successful [45] minority transport has been demonstrated. This forms an innovative avalanche photo-diode in which carriers a generated in a III–V material, and the minority carriers are transported into Silicon for avalanche multiplication. Likewise, we anticipate the successful transport of minority carrier spin across the InP–Si interface.

Thus, the contemplated design of the quantum repeater in Fig. 29 includes InGaAs–InP QWs for the front end, and Si-Ge QWs for the storage and quantum logic gates. The photo-diode and the single photon light emitting diode (LED) are the inverse of one another, so they have almost an identical structure. The only difference is that the photo-diode active region is a sizeable QW, while the single photon LED is a tiny quantum dot. The reason for this asymmetry is that the diffusive transport of a photo-generated electron spin to a potential well trap can take place in picoseconds, during which brief time very little dephasing can occur. By contrast, light emission requires about 1 ns, during which time some dephasing would occur if the electron spin were allowed to wander among different electron spatial wave functions. Furthermore the quantum dot must be small enough to reject a second or third electron to ensure single photon emission. Thus, the emissive QW must indeed be a quantum dot.

Since the exact moment of light emission and light absorption can never be known, it is important for the light emitter and photodetector to be made of material with a similar g-factor, or precession frequency. Then whatever precession angle is lost on emission, would be made up at the absorption end.

A similar problem occurs for transfer across the III–V/Silicon interface. In this case, the g-factor in Silicon is very different from that in the InGaAs semiconductor. Thus, the transfer across the III–V/Silicon interface must be accurately synchronized by timed positive voltage pulses repeating at microwave frequencies, that attract the electron into isotopically purified Si–Ge for safe storage. Statistical fluctuations in the instant of transfer could be responsible for dephasing.

Once the electron is safely stored in the the Si–Ge alloy system, it must be kept a reasonable distance away from other electrons to minimize the disturbance caused by classical dipolar hyperfine coupling that falls off as only $1/r^3$. This can be reasonably accomplished by spacing the electrons by $\geq$100 nm.

Quantum efficiency in the light detection and emission is important. A single QW can be expected to absorb only 1% of normally incident light. Standard techniques can be used to raise this quantum efficiency to near unity, such as cavity enhanced photodetection. A cavity finesse of 100 may be enough for good for a high quantum efficiency photodetector. Likewise in single-photon spontaneous emission, there is a need for efficient mode coupling to a wave-guide mode. This can also be accomplished by a small optical cavity to capture [46] the spontaneous emission, but more easily by shaping the Si–Ge substrate into a hemisphere. Such a hemisphere is known [47] to capture 98% of the emitted radiation. An efficient lens system can then match the point source hemispherical radiation into a single mode optical fiber.

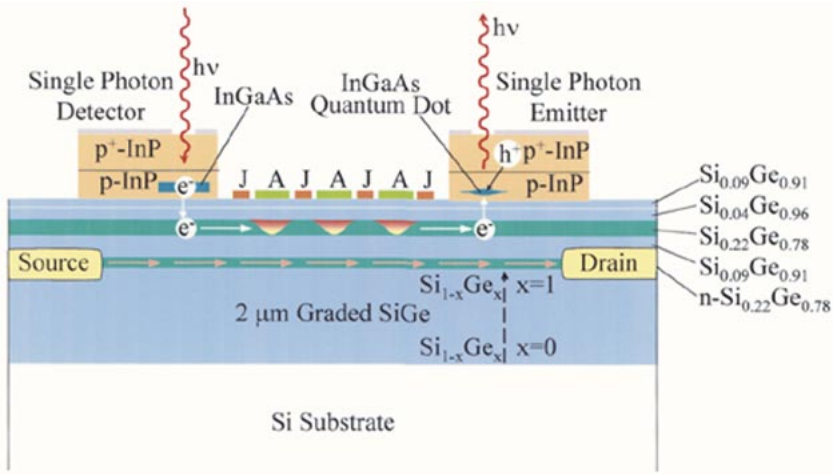


**Fig. 29.** A conceptual cross-sectional diagram of a optical communications quantum repeater chip. A III–V photodetector and single photon light emitting diode would be integrated on a Si–Ge substrate by wafer fusion. A photo-electron spin would be transferred across the hetero-interface and stored in electrostatic traps in SiGe QWs. There the electron spins would undergo the three logic gate operations that are required for quantum teleportation. The resulting electron spin qubit would then be transferred back across the hetero-interface and into the light emitting diode.

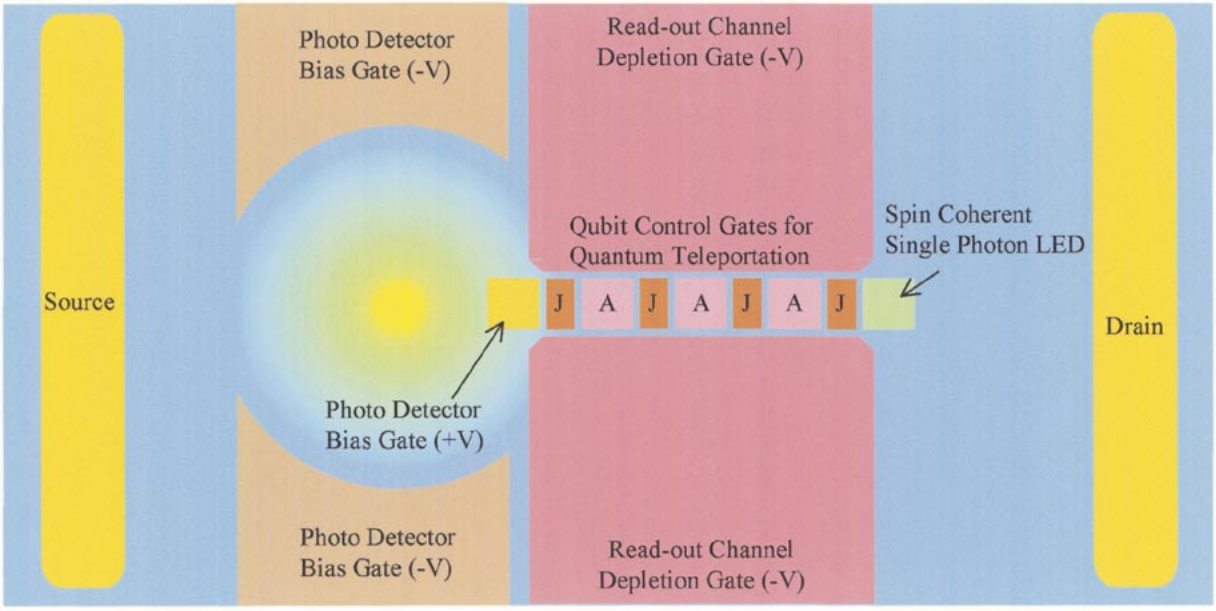


**Fig. 30.** Top view of the quantum repeater of Fig. 29, showing the pinch-off gates, the A and J logic gates, the sizeable photodetector, and the very small single photon light emitting diode. The source/drain channel is used for spin state readout.

A top view of our quantum repeater design is illustrated in Fig. 30. The photodetector is a large circular area to capture the incident radiation, but the photo-electron rapidly diffuses to a potential well under a positive gate for intermediate storage times. Conversely the single-photon LED is a tiny quantum dot that can electro-statically store at most one electron before recombination. The large depletion gates at the top and bottom of Fig. 30 pinch off a narrow channel that resides under the qubit electrodes. In a nomenclature introduced [8] by Kane, the A-gates store the qubits, while the J-gates control their mutual exchange interaction. The pinched off channel under the qubits can be fully polarized by a magnetic field at low temperatures. Those polarized electrons can then be useful for measuring qubit spin flips by the spin-dependent tunneling mechanism, or by the singlet formation mechanism.

The creation of the full quantum repeater illustrated in Figs. 29 and 30 is yet some time away. The individual components have not been fully demonstrated yet. For example, readout of a single electron spin state has not yet been demonstrated. Single photons have been detected [42], and single photons have been emitted [13], but neither with good quantum efficiency. Gate-controlled exchange entanglement of two electrons has not been demonstrated, nor has the resulting spin flip been measured. There are currently many competing research groups working in these areas. Undoubtedly each of these components will be either demonstrated, or further perfected in the near

future. The most difficult challenge may lie in the material and device integration of the five components required in a quantum repeater, even after each component has already been demonstrated individually.

## ACKNOWLEDGMENT

The authors would like to thank K. Holczer for providing them with the spin-echo data for electrons in Silicon in Figs. 2 and 3.

## REFERENCES

[1] P. W. Shor, "Polynomial-time algorithms for prime factorizations and discrete logarithms on a quantum computer," *SIAM J. Computing*, vol. 26, pp. 1484–1509, 1997.

[2] C. H. Bennett, G. Brassard, C. Crepeau, R. Jozsa, A. Peres, and W. K. Wooters, "Teleportation of an unknown quantum state, via dual classical and Einstein-Podolsky-Rosen channels," *Phys. Rev. Lett.*, vol. 70, p. 1895, 1993.

[3] S. J. van Enk, J. I. Cirac, and P. Zoller, "Ideal quantum communication over noisy channels: a quantum optical implementation," *Phys. Rev. Lett.*, vol. 78, p. 4293, 1997.

[4] P. W. Shor, "Scheme for reducing decoherence in quantum computer memory," *Phys. Rev. A*, vol. 52, no. 4, pp. R2493–R2496, Oct. 1995.

[5] D. Kielpinski, V. Meyer, M. A. Rowe, C. A. Sackett, W. M. Itano, C. Monroe, and D. J. Wineland, "A decoherence-free quantum memory using trapped ions," *Science*, vol. 291, pp. 1013–1015, 2001.

[6] L. M. K. Vandersypen, M. Steffen, G. Breyta, C. S. Yannoni, M. H. Sherwood, and I. L. Chuang, "Experimental realization of Shor's quantum factoring algorithm using nuclear magnetic resonance," *Nature*, vol. 414, no. 6866, pp. 883–887, Dec. 20–27, 2001.

[7] D. P. DiVincenzo, D. Bacon, J. Kempe, G. Burkard, and K. B. Whaley, "Universal quantum computation with the exchange interaction," *Nature*, vol. 408, no. 6810, pp. 339–342, Nov. 16, 2000.

[8] B. E. Kane, "A silicon based nuclear spin quantum computer," *Nature*, vol. 393, p. 133, 1998.

[9] J. P. Gordon and K. D. Bowers, "Microwave spin echoes from donor electrons in silicon," *Phys. Rev. Lett.*, vol. 1, p. 368, 1958.

[10] A.M. Tyryshkin, S.A. Lyon, A. V. Astashkin, and A. M. Raitsimring, "Electron spin relaxation times of phosphorous donors in silicon," *Phys. Rev. Lett.*, submitted for publication.

[11] D. Vion, A. Aassime, A. Cottet, P. Joyez, H. Pothier, C. Urbina, D. Esteve, and M. H. Devoret, "Manipulating the quantum state of an electrical circuit," *Science*, vol. 296, pp. 886–889, 2002.

[12] Quantum computation with coherent states, linear interactions, and superposed resources, T. C. Ralph, W. J. Munro, and G. J. Milburn.*http://xxx.arxiv.org/abs/quant-ph/0 110 115* [Online]

[13] C. Santori, M. Pelton, G. Solomon, Y. Dale, and Y. Yamamoto, "Triggered single photons from a quantum dot," *Phys. Rev. Lett.*, vol. 86, no. 8, pp. 1502–1505, Feb., 19 2001.

[14] E. L. Hahn, "Spin echoes," *Phys. Rev.*, vol. 80, pp. 580–594, 1950.

[15] D. D. Awschalom and J. M. Kikkawa, "Electron spin and optical coherence in semiconductors," *Phys. Today*, vol. 52, no. 6, pp. 33–38, June 1999.

[16] J. Preskill, "Reliable quantum computers," in *Proc. Roy. Soc. London*, vol. 454, 1998, pp. 385–410.

[17] T. Szkopek, H.D. Robinson, and E. Yablonovitch, "Comparing Si and GaAs as hosts for electron spin Qubits," to be submitted.

[18] A. V.Alexander V. Khaetskii, D.Daniel Loss, and L.Leonid Glazman, "Electron spin decoherence in quantum dots due to interaction with nuclei," *Phys. Rev. Lett.*, vol. 88, p. 186 802, 2002.

[19] B. E. Kane and M. Pepper, private communication.

[20] R. Vrijen, L. Yablonovitch, K.Kang Wang, H. W.Hong Wen Jiang, A. Balandin, V. Roychowdhury, T. Mor, and D. DiVincenzo, "Electron-spin-resonance transistors for quantum computing in silicon-germanium heterostructures," *Phys. Rev. A*, vol. 62, no. 1, pp. 012 306/1–012 306/10, July 2000.

[21] S. Datta and B. Das, "Electronic analog of the electro-optic modulator," *Appl. Phys. Lett.*, vol. 56, no. 7, pp. 665–667, Feb. 12, 1990.

[22] Y. Kato, R. C. Myers, D. C. Driscoll, A. C. Gossard, J. Levy, and D. D. Awschalom, "Gigahertz electron spin manipulation using g-tensor modulation," *Science*, vol. 299, pp. 1201–1204, 2003.

[23] H. Kosaka, A. A. Kiselev, F. A. Baron, K. W.Ki Wook Kim, and E. Yablonovitch, "Electron g factor engineering in III-V semiconductors for quantum communications," *Electron. Lett.*, vol. 37, no. 7, pp. 464–465, Mar. 29, 2001.

[24] A. A. Kiselev, K. W. Kim, and E. Yablonovitch, "In-plane light-hole $g$ factor in strained cubic heterostructures," *Phys. Rev. B*, vol. 64, p. 125 303, 2001.

[25] H. W. Jiang and E. Yablonovitch, "Gate-controlled electron spin resonance in $\mathbf{GaAs/Al_xGa_{1-x}/As}$ heterostructures," *Phys. Rev. B*, vol. 64, no. 4, p. 041 307, July 15, 2001.

[26] G. Salis, Y. Kato, K. Ensslin, D. C. Driscoll, A. C. Gossard, and D. D. Awschalom, "Electrical control of spin coherence in semiconductor nanostructures," *Nature*, vol. 414, no. 6864, pp. 619–622, Dec. 6, 2001.

[27] M. Dobers, K. v. Klitzing, and G. Weimann, "Electron-spin resonance in the two-dimensional electron gas of $\mathrm{GaAs/Al_xGa_{1-x}As}$ heterostructure," *Phys. Rev. B*, vol. 38, p. 5453, 1988.

[28] "Reports on Progress in Physics," IOP, London, U.K., vol. 64, June 2001.

[29] J. Wrachtrup and A. Gruber, *Solid State NMR*, vol. 11, pp. 59–64, 1998.

[30] C. Durkan and M. E. Wellan, "Electronic spin detection in molecules using scanning-tunneling-microscopy-assisted electron-spin resonance," *Appl. Phys. Lett*, vol. 80, no. 458, 2002.

[31] D. T. Cory, private communication.

[32] F. Jelezko, I. Popa, A. Gruber, C. Tietz, J. Wrachtrup, A. Nizovtsev, and S. Kilin, "Single spin states in a defect center resolved by optical spectroscopy," *Appl. Phys. Lett.*, vol. 81, pp. 2160–2162, 2002.

[33] D. Loss and D. P. DiVincenzo, "Quantum computation with quantum dots," *Phys. Rev.*, vol. A57, p. 120, 1998.

[34] H. Robinson, T. Szkopek, and E. Yablonovitch, "Rapid electron spin rotation by electrostatically tuned anisotropic g-tensor," to be submitted.

[35] D. P. DiVincenzo, D. Bacon, J. Kempe, G. Burkard, and K. B. Whaley, "Universal quantum computation with the exchange interaction," *Nature*, vol. 408, no. 6810, pp. 339–342, Nov. 16, 2000.

[36] J. Kim, O. Benson, H. Kan, and Y. Yamamoto, "A single-photon turnstile device," *Nature*, vol. 397, p. 500, 1999.

[37] C. H. Bennett, G. Brassard, S. Breidbart, and S. Wiesner, "Eavesdrop-detecting quantum communications channel," *IBM Tech. Disclosure Bull.*, vol. 26, pp. 4363–4366, 1984.

[38] J. I. Cirac, P. Zoller, H. J. Kimble, and H. Mabuchi, *Phys. Rev. Lett.*, vol. 78, p. 3221, 1997.

[39] R. Vrijen and E. Yablonovitch, "A spin-coherent semiconductor photodetector for quantum communication," in *Physica E*: Elsevier, June 2001, vol. 10, pp. 569–575.

[40] A.Albert Rose, *Concepts in Photoconductivity and Allied Problems*, Rev. ed. Huntington, N.Y.: Krieger, 1978.

[41] M. J. Kurten and M. J. Uren, "Noise in solid state microstructures: A new perspective on individual defects, interface states, and low-frequency 1/f noise," *Adv. Phys.*, vol. 38, p. 367, 1989.

[42] H. Kosaka, D. S. Rao, H. D. Robinson, P. Bandaru, T. Sakamoto, and E. Yablonovitch, "Photoconductance quantization in a single-photon detector," *Phys. Rev. B (Condensed Matter and Materials Physics*, vol. 65, no. 20, pp. 201 307/1–201 307/4, May 15, 2002.

[43] H. Kosaka, D. S. Rao, H. D. Robinson, P. Bandaru, K. Makita, and E. Yablonovitch, "Single photoelectron trapping, storage, and detection in a field effect transistor," *Phys. Rev. B*, vol. 67, p. 045104, 2003.

[44] I. Malajovich, J. M. Kikkawa, D. D. Awschalom, J. J. Berry, and N. Samarth, "Coherent transfer of spin through a semiconductor heterointerface," *Phys. Rev. Lett.*, vol. 84, no. 5, pp. 1015–1018, Jan., 31 2000.

[45] A. R. Hawkins, T. E. Reynolds, D. R. England, D. I. Babic, M. J. Mondry, K. Streubel, and J. E. Bowers, "Silicon heterointerface photodetector," *Appl. Phys. Lett.*, vol. 68, pp. 3692–3694, 1996.

[46] G. S. Solomon, M. Pelton, and Y. Yamamoto, "Single-mode spontaneous emission from a single quantum dot in a three-dimensional microcavity," *Phys. Rev. Lett.*, vol. 86, no. 17, pp. 3903–3906, Apr. 23, 2001.

[47] W. N. Carr and G. E. Pittman, *Appl. Phys. Lett.*, vol. 3, p. 173, 1963.

[48] D. Gottesman, "Class of quantum error-correcting codes saturating the quantum hamming bound," *Phys. Rev. A*, vol. 54, no. 3, pp. 1862–1868, Sept. 1996.

[49] M. Chiba and A. Hirai, "Electron spin echo behavior of phosphorus doped silicon," *J. Phys. Soc. Japan*, vol. 33, p. 730, 1972.
[50] A. A. Kiselev, K. W. Kim, and E. Yablonovitch, "Designing a heterostructure for the quantum receiver," *Appl. Phys. Lett.*, vol. 80, no. 16, pp. 2857–2859, APR 22, 2002.
[51] T. Pellizari, *Phys. Rev. Lett.*, vol. 79, p. 5242, 1997.
[52] S. J. van Enk, J. I. Cirac, and P. Zoller, *Phys. Rev. Lett.*, vol. 78, p. 4293, 1997.

**Eli Yablonovitch** (Fellow, IEEE) received the Ph.D. degree in applied physics from Harvard University, Cambridge, MA, in 1972.

He worked for two years at Bell Telephone Laboratories, and then became a Professor of Applied Physics at Harvard. In 1979, he joined Exxon to do research on photovoltaic solar energy. Then, in 1984, he joined Bell Communications Research, where he was a Distinguished Member of Staff, and also Director of Solid-State Physics Research. In 1992, he joined the University of California, Los Angeles, where he is Professor of Electrical Engineering.

Dr. Yablonovitch is a Fellow of the Optical Society of America, and the American Physical Society and a Life Member of Eta Kappa Nu. http://www.ee.ucla.edu/faculty/bios/yablonovitch.htm.

**H. W. Jiang**. received the B.S. degree from California State University, Northridge, and the Ph.D. degree from Case Western Reserve University, Cleveland, OH, in 1989.

He is now Professor of Physics at The University of California, Los Angeles. His group's research is centered on exploring new phenomena of low-dimensional semiconductor systems. Another research area is to develop a fundamental building blocks for quantum computation and quantum information processing in advanced semiconductor heterostructures, called spin-resonance-transistors. He has performed experiments at the National High Magnetic Field Laboratory at Florida, and at the Los Alamos National Laboratory, New Mexico.

Among Dr. Jinag's honors are the 1993 William L. McMillan Award for Outstanding Contributions in Condensed Matter Physics; The 1996 Overseas Chinese Physics Association Outstanding Young Researcher Award; and Alfred P. Sloan Fellow 1992–1994.

**Hideo Kosaka** is an Assistant Manager at NEC Fundamental Research Labs, NEC Corporation, Ibaraki, Japan. He was a Visiting Research Engineer for Prof. E. Yablonovitch at the University of California, Los Angeles (UCLA), from July 2000 to June 2002. He then returned to the Fundamental Research laboratories at NEC, Japan. During his stay at UCLA, he fabricated a single-photoelectron transistor that transfers information from a photon to an electron and stores the electron. His expertise is photoelectronic devices and physics especially VCSEL-based smart pixels, photonic crystals, and spin-preserving single-photon detectors used for quantum communications and cryptography.

**Hans D. Robinson**. (Member, IEEE) received the degrees of Licence and Maîtrise in physics from the Ecole Normale Supérieure, Lyon, France, in 1993 and 1994, respectively. He received the Ph.D. degree in physics from Boston University, Boston, MA, in 2000.

His research has included optical spectroscopy and microscopy at low temperatures, in particular near-field microscopy probing the physics of quantum dots. He is currently at the University of California, Los Angeles, where his research is focused electron spin-based quantum computation and communication.

**Deepak Sethu Rao** received the B.E. degree in electrical engineering from Birla Institute of Technology and Science, Pilani, India in 1998. He received the M.S. degree in electrical engineering from the University of California, Los Angeles (UCLA), where he is currently pursuing the Ph.D. degree with Prof. Eli Yablonovitch.

He was with the Broadband Networks facility of Northern Telecom, Bangalore, India, from 1998 to 1999.

**T. Szkopek** received the B.A.Sc and M.A.Sc. degrees from the University of Toronto, Toronto, ON, Canada, in 1999 and 2001 following research on fiber optic gratings and fiber lasers. He is presently working towards the Ph.D. degree under the direction of Prof. Yablonovitch at the University of California, Los Angeles, where he is undertaking research in single electron spin measurement.